Rarefied gas flow over an in-line array of circular cylinders

Taguchi, Satoshi

Charrier, Pierre

(Citation)
Physics of Fluids,20(6):067103-067103

(Issue Date)
2008-06-24

(Resource Type)
journal article

(Version)
Version of Record

Rarefied gas flow over an in-line array of circular cylinders

Satoshi Taguchi[1,a)] and Pierre Charrier[2,b)]
[1]*Organization of Advanced Science and Technology, Kobe University, Kobe 657-8501, Japan*
[2]*Mathématiques Appliquées, Université de Bordeaux, UMR 5251, Bordeaux F-33000, France*

(Received 24 December 2007; accepted 5 May 2008; published online 24 June 2008)

A steady rarefied gas flow through periodic porous media kept at a uniform temperature is considered on the basis of the Bhatnagar–Gross–Krook equation and the diffuse reflection condition on the solid boundary. Under the assumption that the period is much smaller than the length scale of variation of the global pressure distribution, a macroscopic fluid model describing the pressure distribution and the mass flux of the gas in the medium is derived by the homogenization previously proposed by Charrier and Dubroca [Multiscale Model. Simul. **2**, 124 (2003)]. The effective diffusion coefficient contained in the model is constructed numerically as a function of the Knudsen number, in the case of the medium consisting of an in-line array of circular cylinders, with the help of the numerical analysis of a rarefied gas flow in an infinite expanse of the cylinder array driven by a uniform small pressure gradient. An application of the model to an isothermal flow in a porous slab induced by a pressure difference is presented. © *2008 American Institute of Physics*.
[DOI: 10.1063/1.2937461]

I. INTRODUCTION

Recently, kinetic theory of gases (or molecular gas dynamics)[1–5] is attracting great attention in connection with microfluidics.[6–9] Flows of rarefied gas induced by the thermal effect, such as the thermal creep flow (thermal transpiration),[10–14] the thermal stress slip flow,[15,16] the nonlinear thermal stress flow,[16,17] and the thermal edge flow,[18,19] have potential applicability as nonmechanical flow controllers in microscale systems. A prototypical thermal pump using the thermal edge flow has been recently fabricated in Ref. 20. On the other hand, the thermal pump using the thermal transpiration, also known as the Knudsen pump (or compressor), has been the subject of a large amount of work.[21–35]

The Knudsen pump is typically a series of narrow and wide pipes connected one after the other, with a periodic temperature distribution along the pipe.[4,5] Because of its practical importance and theoretical interest, the flow and the pumping effect for this Knudsen pump have been extensively investigated and many successful results have been obtained both theoretically[24,28,33,34] and experimentally.[27,29,30] The applicability of the Knudsen pump to a gas separator has been numerically demonstrated in Ref. 35.

Meanwhile, another type of pumping device was proposed by Kayashima[36] on the basis of the same idea as the Knudsen pump. He proposed to use porous media, whose pore sizes are of the same order as the mean free path of the gas molecules, in place of the pipes. This pumping device using porous media seems to be as attractive as the Knudsen pump using pipes, since we can benefit not only from the thermal creep flow but also from other thermally driven flows, by devising the pore geometries. However, because of its geometrical complexity, no result has been reported for this device so far. For practice purpose, it would be very useful if we have a simple macroscopic model to describe the global flow field in porous media, as in the case of the original Knudsen pump.[33,34]

In this paper, as a first step toward the theoretical assessment of the Kayashima's device, we try to derive such a macroscopic model, called the fluid model here, on the basis of kinetic theory for a porous medium consisting of an in-line array of circular cylinders. As the basic kinetic equation, we employ the Bhatnagar–Gross–Krook (BGK) equation[37–39] and assume the diffuse reflection condition on the boundary. In addition, in order to simplify the analysis and to concentrate on the numerical results we obtained, we consider here the isothermal case, i.e., the temperature of the solid boundary is uniform throughout the medium. The inclusion of the thermal effect is necessary for the full analysis of the pumping effect. However, it is straightforward and will be treated in a subsequent paper.

In Sec. II, we consider a rarefied gas in a periodic porous medium kept at a uniform temperature and derive a macroscopic equation that describes the global (steady) pressure distribution and the mass-flow rate by a systematic analysis of the kinetic system. Here, for possible future extension, the formal analysis is carried out for the general periodic structure not limited to the in-line array of circular cylinders. As a method of analysis, we adopt the homogenization technique introduced by Charrier and Dubroca.[40] Here, our basic assumption for the derivation is the smallness of the period compared to the length scale of variation of the global pressure distribution.

The derived model contains a diffusion tensor whose components are essentially given by the mass-flow rates (in the unit cell) of a flow induced in an infinite expanse of the periodic structure by a uniform pressure gradient. Therefore, Sec. III is devoted to the numerical analysis of a steady rarefied gas flow over an in-line array of circular cylinders driven by a small uniform pressure gradient. We obtain nu-

[a)]Electronic mail: taguchi@mech.kobe-u.ac.jp.
[b)]Electronic mail: pierre.charrier@math.u-bordeaux1.fr.

merically the mass-flow rate as a function of the Knudsen number. This completes the derivation of the macroscopic fluid model.

Finally, in Sec. IV, we show a simple application of the fluid model to an isothermal flow in a porous slab made of an in-line array of cylinders, whose two ends are maintained at different pressures.

II. FLUID MODEL FOR RAREFIED GAS FLOWS IN POROUS MEDIA WITH PERIODIC STRUCTURE

A. Problem and basic equations

1. Problem

We consider a rarefied gas in a porous medium with periodic structure with a period ℓ. The solid phase is kept at a uniform and constant temperature T_0 and the gas is driven by the pressure gradient. Let us denote the length scale of variation of the global pressure distribution by L. We investigate the steady behavior of the gas under the following assumptions:

(i) The behavior of the gas is described by the BGK model.
(ii) The gas molecules are reflected diffusely on the solid boundary.
(iii) The period ℓ is much smaller than the length scale of variation of the overall pressure distribution L, i.e., $\ell \ll L$.

For the sake of clarity, we suppose that there is no isolated pore so that there is no confinement of the gas inside a pore.

2. Basic equations

Let p_* denote the reference pressure, R the specific gas constant, $\rho_* = p_*/RT_0$ the reference density, $L\mathbf{x}$ (or Lx_i) the space rectangular coordinates, $(2RT_0)^{1/2}\boldsymbol{\zeta}$ [or $(2RT_0)^{1/2}\zeta_i$] the molecular velocity, $\rho_*(2RT_0)^{-3/2}\hat{f}(\mathbf{x},\boldsymbol{\zeta})$ the distribution function, $\rho_*\hat{\rho}$ the density, $(2RT_0)^{1/2}\hat{\mathbf{v}}$ [or $(2RT_0)^{1/2}\hat{v}_i$] the flow velocity, $T_0\hat{T}$ the temperature, and $p_*\hat{p}$ the pressure of the gas. Let us denote by D_f the region inside the porous medium occupied by the gas in the dimensionless $\mathbf{x}$ space. The BGK equation is written in the following dimensionless form:

$$\boldsymbol{\zeta}\cdot\nabla_x\hat{f} = \frac{2}{\sqrt{\pi}}\frac{1}{K_*\epsilon}\hat{\rho}(\hat{f}_e - \hat{f}) \quad (\mathbf{x}\in D_f), \tag{1}$$

$$\hat{f}_e = \frac{\hat{\rho}}{(\pi\hat{T})^{3/2}}\exp\left(-\frac{|\boldsymbol{\zeta}-\hat{\mathbf{v}}|^2}{\hat{T}}\right), \tag{2}$$

$$\hat{\rho} = \int \hat{f}\,d\boldsymbol{\zeta}, \tag{3a}$$

$$\hat{\mathbf{v}} = \frac{1}{\hat{\rho}}\int \boldsymbol{\zeta}\hat{f}\,d\boldsymbol{\zeta}, \tag{3b}$$

$$\hat{p} = \hat{\rho}\hat{T} = \frac{2}{3}\int |\boldsymbol{\zeta}-\hat{\mathbf{v}}|^2\hat{f}\,d\boldsymbol{\zeta}, \tag{3c}$$

$$\epsilon = \frac{\ell}{L}, \quad K_* = \frac{\ell_*}{\ell}. \tag{4}$$

where ∇_x is the gradient operator with respect to $\mathbf{x}$ and $d\boldsymbol{\zeta} = d\zeta_1 d\zeta_2 d\zeta_3$. Here and in what follows, the domain of integration with respect to $\boldsymbol{\zeta}$ is the whole space unless the contrary is stated. ϵ is the ratio of the period to the global length scale of variation, ℓ_* is the mean free path of the gas molecules in the equilibrium state at rest with density ρ_* and temperature T_0, and K_* is the Knudsen number based on the period. For the BGK model, ℓ_* is given by $\ell_* = (2/\sqrt{\pi})\times(2RT_0)^{1/2}/A_c\rho_*$, where A_c is a constant ($A_c\rho_*$ is the collision frequency in the reference equilibrium state, which is independent of the molecular speed).[5] ℓ_* is related to the corresponding viscosity μ_* by $\mu_* = (\sqrt{\pi}/2)p_*(2RT_0)^{-1/2}\ell_*$.

Let A_{fs} denote the surface of the solid phase (in the dimensionless $\mathbf{x}$ space). The diffuse reflection condition on the solid boundary is given by

$$\hat{f} = \hat{\sigma}_w E(\boldsymbol{\zeta}) \quad \text{for } \boldsymbol{\zeta}\cdot\mathbf{n} > 0 \quad (\mathbf{x}\in A_{fs}), \tag{5}$$

with

$$E(\boldsymbol{\zeta}) = \pi^{-3/2}\exp(-|\boldsymbol{\zeta}|^2), \tag{6}$$

$$\hat{\sigma}_w(\mathbf{x}) = -2\sqrt{\pi}\int_{\boldsymbol{\zeta}\cdot\mathbf{n}<0} \boldsymbol{\zeta}\cdot\mathbf{n}\hat{f}(\mathbf{x},\boldsymbol{\zeta})\,d\boldsymbol{\zeta}, \tag{7}$$

where $\mathbf{n}$ (or n_i) is the unit normal vector to A_{fs} pointed to the gas. It should be noted that the diffuse reflection condition [Eq. (5) with Eq. (7)] implies that there is no net mass flux across the interface (impermeability condition), i.e.,

$$\int \boldsymbol{\zeta}\cdot\mathbf{n}\hat{f}(\mathbf{x},\boldsymbol{\zeta})\,d\boldsymbol{\zeta} = 0 \quad (\mathbf{x}\in A_{fs}). \tag{8}$$

Suppose that the geometrical configuration of the unit cell is specified. Then, the present system is characterized by the following dimensionless parameters:

$$\epsilon = \frac{\ell}{L}, \quad K_* = \frac{\ell_*}{\ell}. \tag{9}$$

ϵ is a small parameter because of the assumption (iii). On the other hand, we assume that K_* is of the order of unity, i.e., $K_* = O(1)$.

B. Homogenization and fluid model

In this subsection, we derive a macroscopic fluid model describing the global pressure distribution inside the periodic porous medium by homogenization. The homogenization method is based on an asymptotic expansion using two length scales, one describing the spatial variation over the global length scale, and the other describing the spatial variation over the length scale characterized by the period. The reader interested in the principal ideas and concepts of the homogenization approach can refer to Ref. 41 and to

Refs. 40 and 42–44 for its application to kinetic models. It should also be mentioned that the homogenization method is used to derive global diffusion models for the Knudsen pump in Refs. 33 and 34.

Now let us start our analysis. Because of the periodicity, the global structure is composed of many unit cells with period ϵ (or ℓ in the dimensional space). We denote by X a basic unit cell fixed in the $\mathbf{x}$ space. Let us introduce the following new variable:

$$\mathbf{y} = (y_1, y_2, y_3) = \frac{\mathbf{x}}{\epsilon}. \tag{10}$$

The variable $\mathbf{x}$ describes the long scale variation over the global length scale, whereas the variable $\mathbf{y}$ corresponds to the short scale variation over the period. We assume that $\hat{f}$ is a function of $\mathbf{x}$, $\mathbf{y}$, and $\boldsymbol{\zeta}$, i.e.,

$$\hat{f} = \hat{f}(\mathbf{x}, \mathbf{y}, \boldsymbol{\zeta}), \tag{11}$$

and that $\hat{f}$ is periodic in $\mathbf{y}$ with period 1. The validity of these assumptions can be verified from the result of analysis. Let us denote by Y the unit cube in the stretched $\mathbf{y}$ space corresponding to the unit cell X, by Y_f the part of Y corresponding to the gas region, and by S the solid boundary in Y. Then, with these new variables, the system (1)–(3), (5), and (7) is recast as

$$\epsilon \boldsymbol{\zeta} \cdot \nabla_x \hat{f} + \boldsymbol{\zeta} \cdot \nabla_y \hat{f} = \frac{2}{\sqrt{\pi}} \frac{1}{K_*} \hat{\rho}(\hat{f}_e - \hat{f}) \quad (\mathbf{x} \in D_f,\ \mathbf{y} \in Y_f), \tag{12}$$

$$\hat{f} = \hat{\sigma}_w E(\boldsymbol{\zeta}) \quad \text{for } \boldsymbol{\zeta} \cdot \mathbf{n} > 0 \quad (\mathbf{x} \in A_{fs},\ \mathbf{y} \in S), \tag{13}$$

$$\hat{\sigma}_w = -2\sqrt{\pi} \int_{\zeta \cdot \mathbf{n} < 0} \boldsymbol{\zeta} \cdot \mathbf{n} \hat{f} d\boldsymbol{\zeta}, \tag{14}$$

$$\hat{f}: \text{ periodic} \quad (\mathbf{y} \in \partial Y_f \cap \partial Y), \tag{15}$$

where ∇_y is the gradient operator with respect to $\mathbf{y}$, $\partial Y_f \cap \partial Y$ is the boundary of Y occupied by the gas, and the range of $\mathbf{y}$ is restricted to Y_f with the periodic condition (15).

We look for a solution $\hat{f}(\mathbf{x}, \mathbf{y}, \boldsymbol{\zeta})$ of the above system (12)–(15) in the form of simple expansion in ϵ, i.e.,

$$\hat{f} = \hat{f}_{(0)} + \hat{f}_{(1)}\epsilon + \hat{f}_{(2)}\epsilon^2 + \cdots. \tag{16}$$

Corresponding to the expansion (16), the macroscopic quantities of the gas $h = h(\mathbf{x}, \mathbf{y})$ ($h = \hat{\rho}, \hat{\mathbf{v}}, \hat{T}, \hat{p}$) are expanded in ϵ as

$$h = h_{(0)} + h_{(1)}\epsilon + h_{(2)}\epsilon^2 + \cdots. \tag{17}$$

The relations between $h_{(m)}$ and $\hat{f}_{(m)}$ ($m = 0, 1, \ldots$) are obtained by substituting the expansions of h and $\hat{f}$ into the definition of the macroscopic quantities, Eqs. (3a)–(3c), and equating the coefficient of the same power of ϵ. We also expand the local Maxwellian $\hat{f}_e$ in ϵ, i.e.,

$$\hat{f}_e = \hat{f}_{e(0)} + \hat{f}_{e(1)}\epsilon + \hat{f}_{e(2)}\epsilon^2 + \cdots. \tag{18}$$

Here, the coefficients $\hat{f}_{e(m)}$ are expressed in terms of $h_{(n)}$ ($n \le m$). If we substitute Eqs. (16)–(18) into the equations and the boundary conditions, and balance order by order in ϵ, we obtain a sequence of problems which can be solved from the lowest order.

1. Zeroth order approximation in ϵ

The equation and the boundary condition for the ϵ^0 order are given by

$$\boldsymbol{\zeta} \cdot \nabla_y \hat{f}_{(0)} = \frac{2}{\sqrt{\pi}} \frac{1}{K_*} \hat{\rho}_{(0)}(\hat{f}_{e(0)} - \hat{f}_{(0)}) \quad (\mathbf{y} \in Y_f), \tag{19}$$

$$\hat{f}_{e(0)} = \frac{\hat{\rho}_{(0)}}{(\pi \hat{T}_{(0)})^{3/2}} \exp\left(- \frac{|\boldsymbol{\zeta} - \hat{\mathbf{v}}_{(0)}|^2}{\hat{T}_{(0)}} \right), \tag{20}$$

$$\hat{f}_{(0)} = \hat{\sigma}_{w(0)} E(\boldsymbol{\zeta}), \quad \boldsymbol{\zeta} \cdot \mathbf{n} > 0 \quad (\mathbf{y} \in S), \tag{21}$$

$$\hat{\sigma}_{w(0)} = -2\sqrt{\pi} \int_{\zeta \cdot \mathbf{n} < 0} \boldsymbol{\zeta} \cdot \mathbf{n} \hat{f}_{(0)} d\boldsymbol{\zeta}, \tag{22}$$

where the system should be supplemented by the periodic boundary condition for $\hat{f}_{(0)}$ on $\partial Y_f \cap \partial Y$. The zeroth order macroscopic quantities of the gas $\hat{\rho}_{(0)}$, $\hat{\mathbf{v}}_{(0)}$, $\hat{T}_{(0)}$, and $\hat{p}_{(0)}$ are related to $\hat{f}_{(0)}$ by the following relations:

$$\hat{\rho}_{(0)} = \int \hat{f}_{(0)} d\boldsymbol{\zeta}, \tag{23a}$$

$$\hat{\mathbf{v}}_{(0)} = \frac{1}{\hat{\rho}_{(0)}} \int \boldsymbol{\zeta} \hat{f}_{(0)} d\boldsymbol{\zeta}, \tag{23b}$$

$$\hat{p}_{(0)} = \hat{\rho}_{(0)} \hat{T}_{(0)} = \frac{2}{3} \int |\boldsymbol{\zeta} - \hat{\mathbf{v}}_{(0)}|^2 \hat{f}_{(0)} d\boldsymbol{\zeta}. \tag{23c}$$

It should be noted that the variable $\mathbf{x}$ appears in the equations only as a parameter.

The solution of this problem is shown to be independent of $\mathbf{y}$ and is given by

$$\hat{f}_{(0)} = \hat{\rho}_{(0)}(\mathbf{x}) E(\boldsymbol{\zeta}) = \frac{\hat{\rho}_{(0)}(\mathbf{x})}{\pi^{3/2}} \exp(-|\boldsymbol{\zeta}|^2), \tag{24}$$

where $\hat{\rho}_{(0)}$ is an undetermined function of $\mathbf{x}$. The proof is analogous to that of Ref. 40 and therefore omitted here. In particular, if we substitute Eq. (24) into Eqs. (23b) and (23c), we obtain

$$\hat{\mathbf{v}}_{(0)} = 0, \quad \hat{T}_{(0)} = 1, \quad \hat{p}_{(0)} = \hat{\rho}_{(0)}. \tag{25}$$

2. First order approximation in ϵ

With the aid of the solution for the zeroth order approximation, our system for the first order approximation becomes

$$\boldsymbol{\zeta} \cdot \nabla_y \hat{f}_{(1)} = \frac{2}{\sqrt{\pi}} \frac{1}{K_*} \hat{\rho}_{(0)}(\hat{f}_{e(1)} - \hat{f}_{(1)}) - \boldsymbol{\zeta} \cdot \nabla_x \hat{f}_{(0)} \quad (\mathbf{y} \in Y_f), \tag{26}$$

$$\hat{f}_{e(1)} = \hat{\rho}_{(0)} E(\boldsymbol{\zeta}) \left[\frac{\hat{\rho}_{(1)}}{\hat{\rho}_{(0)}} + 2\hat{\mathbf{v}}_{(1)} \cdot \boldsymbol{\zeta} + \left(|\boldsymbol{\zeta}|^2 - \frac{3}{2} \right) \hat{T}_{(1)} \right], \tag{27}$$

$$\hat{f}_{(1)} = \hat{\sigma}_{w(1)} E(\boldsymbol{\zeta}), \quad \boldsymbol{\zeta} \cdot \mathbf{n} > 0 \quad (\mathbf{y} \in S), \tag{28}$$

$$\hat{\sigma}_{w(1)} = -2\sqrt{\pi} \int_{\boldsymbol{\zeta}\cdot\mathbf{n}<0} \boldsymbol{\zeta} \cdot \mathbf{n} \hat{f}_{(1)} d\boldsymbol{\zeta}. \tag{29}$$

The above system should be supplemented by the periodic boundary condition for $\hat{f}_{(1)}$ on $\partial Y_f \cap \partial Y$. Here, it is noted that Eq. (26) is the linearized BGK equation with the inhomogeneous term $-\boldsymbol{\zeta} \cdot \nabla_x \hat{f}_{(0)} = -\boldsymbol{\zeta} \cdot \nabla_x \hat{p}_{(0)} E(\boldsymbol{\zeta})$. The first order macroscopic quantities of the gas are given by

$$\hat{\rho}_{(1)} = \int \hat{f}_{(1)} d\boldsymbol{\zeta}, \tag{30a}$$

$$\hat{\mathbf{v}}_{(1)} = \frac{1}{\hat{\rho}_{(0)}} \int \boldsymbol{\zeta} \hat{f}_{(1)} d\boldsymbol{\zeta}, \tag{30b}$$

$$\hat{p}_{(1)} = \hat{\rho}_{(0)} \hat{T}_{(1)} = \frac{2}{3} \int \left(|\boldsymbol{\zeta}|^2 - \frac{3}{2} \right) \hat{f}_{(1)} d\boldsymbol{\zeta}. \tag{30c}$$

The solution to the problem (26)–(29) can be expressed in the following form:

$$\hat{f}_{(1)} = \hat{f}_{(0)} \left[\frac{\langle \hat{p}_{(1)} \rangle^f}{\hat{p}_{(0)}} + \boldsymbol{\Phi}(\mathbf{y}, \boldsymbol{\zeta}; K_0(\mathbf{x})) \cdot \nabla_x \ln \hat{p}_{(0)} \right], \tag{31}$$

where $\langle \hat{p}_{(1)} \rangle^f$ is the average of $\hat{p}_{(1)}$ with respect to $\mathbf{y}$ over the fluid part Y_f and is an undetermined function of $\mathbf{x}$, K_0 is a kind of local Knudsen number defined by

$$K_0(\mathbf{x}) = \frac{K_*}{\hat{p}_{(0)}(\mathbf{x})} = \frac{K_*}{\hat{\rho}_{(0)}(\mathbf{x})}, \tag{32}$$

and the vector function $\boldsymbol{\Phi}$ (or Φ^i) depending on $\mathbf{y}$ and $\boldsymbol{\zeta}$ is the solution of the following boundary-value problem:

$$\boldsymbol{\zeta} \cdot \nabla_y \Phi^i = \frac{2}{\sqrt{\pi}} \frac{1}{K_0} \hat{L}_{\mathrm{BGK}}(\Phi^i) - \zeta_i \quad (\mathbf{y} \in Y_f), \tag{33}$$

$$\Phi^i = \kappa_w^i \quad \text{for } \boldsymbol{\zeta} \cdot \mathbf{n} > 0 \quad (\mathbf{y} \in S), \tag{34}$$

$$\kappa_w^i = -2\sqrt{\pi} \int_{\boldsymbol{\zeta}\cdot\mathbf{n}<0} \boldsymbol{\zeta} \cdot \mathbf{n} \Phi^i E(\boldsymbol{\zeta}) d\boldsymbol{\zeta}, \tag{35}$$

Φ^i: periodic $\quad (\mathbf{y} \in \partial Y_f \cap \partial Y)$,

subsidiary condition: (36)

$$\int_{Y_f} \int \Phi^i E(\boldsymbol{\zeta}) d\boldsymbol{\zeta} d\mathbf{y} = 0. \tag{37}$$

Here, $\hat{L}_{\mathrm{BGK}}$ is the linearized BGK collision operator defined by

$$\hat{L}_{\mathrm{BGK}}(g) = \int \left[1 + 2\boldsymbol{\zeta} \cdot \boldsymbol{\zeta}_* + \frac{2}{3} \left(|\boldsymbol{\zeta}|^2 - \frac{3}{2} \right) \left(|\boldsymbol{\zeta}_*|^2 - \frac{3}{2} \right) \right] \times g(\boldsymbol{\zeta}_*) E(\boldsymbol{\zeta}_*) d\boldsymbol{\zeta}_* - g, \tag{38}$$

where g is a function of $\boldsymbol{\zeta}$. It should be noted that $\boldsymbol{\Phi}$ depends not only on the geometry of the unit cell but also on $\mathbf{x}$ through K_0. Its dependence on $\mathbf{x}$ is explicitly shown in Eq. (31).

The solution Φ^i to Eqs. (33)–(37) corresponds to the solution of an elemental flow problem of rarefied gases associated with periodic porous media, i.e., the flow induced in a periodically structured matrix (with a uniform temperature) when there is a (small) uniform pressure gradient applied in the y_i direction. The problem may be called the cell auxiliary problem (Ref. 40).

With the aid of the expression for $\hat{f}_{(1)}$, one can compute the macroscopic quantities corresponding to the first order approximation from Eqs. (30a)–(30c). The results are given by

$$\hat{\rho}_{(1)} = \langle \hat{p}_{(1)} \rangle^f + \boldsymbol{\omega} \cdot \nabla_x \hat{p}_{(0)}, \tag{39a}$$

$$\hat{\mathbf{v}}_{(1)} = \mathbf{u} \nabla_x \ln \hat{p}_{(0)}, \tag{39b}$$

$$\hat{T}_{(1)} = \boldsymbol{\tau} \cdot \nabla_x \ln \hat{p}_{(0)}, \tag{39c}$$

$$\hat{p}_{(1)} = \langle \hat{p}_{(1)} \rangle^f + \mathbf{P} \cdot \nabla_x \hat{p}_{(0)}, \tag{39d}$$

where the vector functions $\boldsymbol{\omega}$ (or ω^i), $\boldsymbol{\tau}$ (or τ^i), and $\mathbf{P}$ (or P^i) are given by

$$\omega^i(\mathbf{y}; K_0) = \int \Phi^i(\mathbf{y}, \boldsymbol{\zeta}; K_0) E(\boldsymbol{\zeta}) d\boldsymbol{\zeta}, \tag{40a}$$

$$\tau^i(\mathbf{y}; K_0) = \frac{2}{3} \int \left(|\boldsymbol{\zeta}|^2 - \frac{3}{2} \right) \Phi^i(\mathbf{y}, \boldsymbol{\zeta}; K_0) E(\boldsymbol{\zeta}) d\boldsymbol{\zeta}, \tag{40b}$$

$$P^i = \omega^i + \tau^i, \tag{40c}$$

and $\mathbf{u}$ is the 3×3 matrix with its (i,j) component given by

$$u_i^j(\mathbf{y}; K_0) = \int \zeta_i \Phi^j(\mathbf{y}, \boldsymbol{\zeta}; K_0) E(\boldsymbol{\zeta}) d\boldsymbol{\zeta}. \tag{41}$$

3. Second order approximation in ϵ and fluid model

Now, we consider the problem for ϵ^2-order approximation. The equation for the second order approximation is as follows:

$$\boldsymbol{\zeta} \cdot \nabla_y \hat{f}_{(2)} = \frac{2}{\sqrt{\pi}} \frac{1}{K_*} [\hat{\rho}_{(0)} (\hat{f}_{e(2)} - \hat{f}_{(2)}) + \hat{\rho}_{(1)} (\hat{f}_{e(1)} - \hat{f}_{(1)})] - \boldsymbol{\zeta} \cdot \nabla_x \hat{f}_{(1)} \quad (\mathbf{y} \in Y_f). \tag{42}$$

Here, the explicit form of $\hat{f}_{e(2)}$ and the boundary condition for $\hat{f}_{(2)}$ on S have been omitted for shortness. Again, the system should be supplemented by the periodic boundary

condition for $\hat{f}_{(2)}$ on $\partial Y_f \cap \partial Y$. In this section, we derive a macroscopic fluid model by considering the necessary condition for the above problem.

We integrate Eq. (42) with respect to $\boldsymbol{\zeta}$ over the whole space and subsequently with respect to $\mathbf{y}$ over the whole domain of Y_f. Since the contribution from the first term on the right-hand side of Eq. (42) vanishes by the former integration, we obtain

$$\nabla_x \cdot \left(\hat{\rho}_{(0)} \int_{Y_f} \hat{\mathbf{v}}_{(1)} d\mathbf{y} \right) + \int_{Y_f} \int \boldsymbol{\zeta} \cdot \nabla_y \hat{f}_{(2)} d\boldsymbol{\zeta} d\mathbf{y} = 0, \tag{43}$$

where $d\mathbf{y} = dy_1 dy_2 dy_3$. Here, we have used the fact that $\hat{\rho}_{(0)}$ is independent of $\mathbf{y}$. It is also noted that the second integral on the left-hand side of Eq. (43) vanishes because of the periodicity of $\hat{f}_{(2)}$ on $\partial Y_f \cap \partial Y$ as well as the impermeability condition

$$\int \boldsymbol{\zeta} \cdot \mathbf{n} \hat{f}_{(2)} d\boldsymbol{\zeta} = 0 \quad (\mathbf{y} \in S), \tag{44}$$

which is derived from the boundary condition for $\hat{f}_{(2)}$ that is not given here [cf. Eq. (8)]. Thus, with the aid of Eq. (39b), Eq. (43) can be rewritten as

$$\nabla_x \cdot (\mathbf{M}_P \nabla_x \hat{p}_{(0)}) = 0, \tag{45}$$

where $\mathbf{M}_P$ (or M_{Pij}) is the 3×3 matrix with its (i,j) component given by

$$M_{Pij}(K_0) = \int_{Y_f} u_i^j(\mathbf{y}; K_0) d\mathbf{y}, \tag{46}$$

and the relation $\hat{\rho}_{(0)} = \hat{p}_{(0)}$ has been used. Equation (46) can be further transformed into the following form:

$$M_{Pij}(K_0) = \int_{S_i} u_i^j(\mathbf{y}; K_0)|_{\mathbf{y} \in S_i} d\mathbf{y}_i, \tag{47}$$

where S_i is a cross section of Y_f perpendicular to the y_i axis and $d\mathbf{y}_i$ is the surface element on S_i, i.e., $(d\mathbf{y}_1, d\mathbf{y}_2, d\mathbf{y}_3) = (dy_2 dy_3, dy_1 dy_3, dy_1 dy_2)$. Thus, M_{Pij} is the dimensionless mass-flow rate in the unit cell in the y_i (or x_i) direction due to the pressure gradient in the y_j (or x_j) direction. It should be noted that M_{Pij} is independent of the way of choosing S_i. It is also noted that $\mathbf{M}_P$ depends on the geometry of the unit cell.

To summarize, the fluid model describing the global behavior of the gas is written in the following form:

$$\nabla_x \cdot \mathbf{M} = 0, \tag{48a}$$

$$\mathbf{M} = \mathbf{M}_P(K_0) \nabla_x \hat{p}_{(0)}, \tag{48b}$$

$$K_0 = \frac{K_*}{\hat{p}_{(0)}}. \tag{48c}$$

Here, $\mathbf{M}$ (or M_i) represents the dimensionless mass-flow rate, i.e., if the dimensional mass-flow rate in the unit cell (per unit time) in the x_i direction is denoted by $\tilde{M}_i$, it is related to M_i by

$$\tilde{M}_i / \ell^2 \rho_* (2RT_0)^{1/2} = \epsilon M_i + O(\epsilon^2). \tag{49}$$

Let us suppose that $\mathbf{M}_P$ is known. Then, Eqs. (48a)–(48c) form a closed set of equations for the leading order pressure $\hat{p}_{(0)}$ and the equation is of elliptic type. If we specify the ambient pressure distribution (its variation may be large) as the boundary condition, Eqs. (48a)–(48c) determine the overall pressure distribution as well as the mass flux in the porous medium.

Equation (48) is similar to the isothermal version of the diffusion equation derived in Ref. 34 for a flow in a narrow pipe. Models in the same spirit have also been derived for unidirectional rarefied gas flows[33,35,45] and applied to microflows.[46–49] On the other hand, the macroscopic models for rarefied gas flows in porous media have been classically derived on the basis of the dusty gas model[50] or more recently on the basis of the modified Boltzmann equations with additional collision terms which take into account the effect of the collisions of the gas molecules with the solid matrix.[51–53] It should be stressed that, in the present approach, the effect of the solid boundary is included in the effective diffusion tensor entirely through the boundary-value problem (or the cell auxiliary problem) for $\boldsymbol{\Phi}$. In this connection, it should be mentioned that, although the diffuse reflection condition is assumed in the present analysis, the extension to more general boundary conditions is straightforward (see, e.g., Ref. 34). In this case, the general form of the fluid model does not change, and the effect of the boundary appears in the diffusion tensor $\mathbf{M}_P$ through the cell auxiliary problem. It should also be mentioned that the diffusion approximations of the kinetic system have been made mathematically rigorous for a collisionless gas; see Refs. 54–57 for the case of channel or pipe and Ref. 58 for the case of circular cylinders in a staggered arrangement.

III. NUMERICAL ANALYSIS OF A RAREFIED GAS FLOW OVER AN IN-LINE ARRAY OF CIRCULAR CYLINDERS DRIVEN BY PRESSURE GRADIENT

In this section, we assume that the porous medium is made of an in-line array of circular cylinders and we carry out an actual numerical analysis to obtain $\mathbf{M}_P$. To be more specific, the problem to determine $\mathbf{M}_P$ (i.e., the cell auxiliary problem) is equivalent to the problem of a steady rarefied gas flow over an in-line array of circular cylinders driven by a small uniform pressure gradient, and $\mathbf{M}_P$ is essentially the mass-flow rate in the unit cell. In this section, we solve this problem numerically to obtain $\mathbf{M}_P$.

A. Formulation of the problem

We begin with the physical description of the problem. Consider a rarefied gas around infinitely many circular cylinders whose centers are located at $(m\ell, n\ell)$ (m, n: integers; $\ell > 0$: constant) in the (Y_1, Y_2) plane, where Y_i is the rectangular coordinate system (Fig. 1). The cylinders are kept at a uniform temperature T_0 and the common radius of the cylinders is denoted by r_c ($r_c/\ell < 0.5$). The gas is subject to a uniform pressure gradient in the Y_1 direction. That is, the pressure of the gas is given by $p_0(1 + C_P Y_1/\ell)$ (p_0, C_P: con-

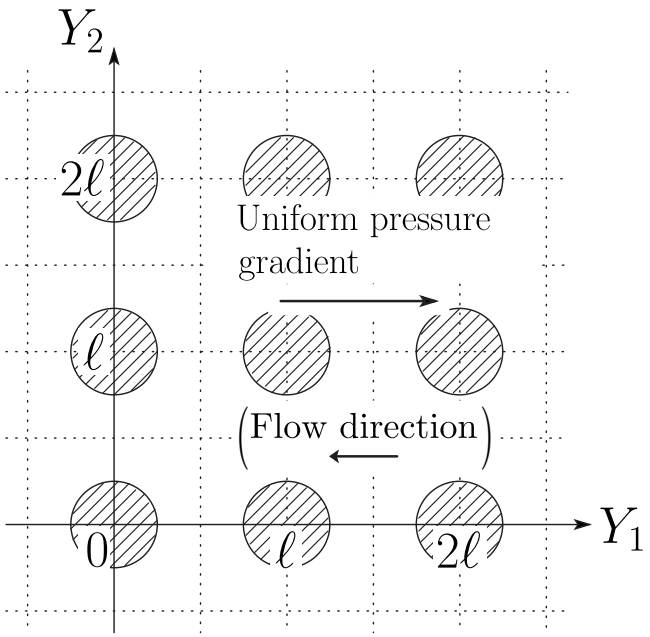

FIG. 1. A rarefied gas flow over an in-line array of circular cylinders induced by a pressure gradient.

stants) in the absence of the cylinders. Investigate the steady behavior of the gas disturbed by the presence of the cylinders under the following assumptions: (i) the behavior of the gas is described by the BGK equation; (ii) the molecules are reflected diffusely on the cylinders; and (iii) the gradient C_P is so small that the equation and the boundary condition can be linearized around the reference equilibrium state at rest with pressure p_0 and temperature T_0.

In this section, we use the dimensionless space coordinates $y_i = Y_i/\ell$ and introduce the following new notations: $\rho_0(2RT_0)^{-3/2}E(\boldsymbol{\zeta})(1+\tilde{\Phi})$ is the velocity distribution function, $\rho_0(1+\tilde{\omega})$ is the density of the gas, $(2RT_0)^{1/2}\tilde{u}_i$ its flow velocity $(\tilde{u}_3=0)$, $T_0(1+\tilde{\tau})$ its temperature, $p_0(1+\tilde{P})$ its pressure, $\rho_0 = p_0/RT_0$ is the reference density, ℓ_0 is the mean free path of the gas molecules at the reference equilibrium state at rest with temperature T_0 and density ρ_0, and $\mathrm{Kn} = \ell_0/\ell$ is the Knudsen number.

The linearized BGK equation for the present steady two-dimensional problem is given by

$$\zeta_1\frac{\partial\tilde{\Phi}}{\partial y_1} + \zeta_2\frac{\partial\tilde{\Phi}}{\partial y_2} = \frac{2}{\sqrt{\pi}}\frac{1}{\mathrm{Kn}}\left[\tilde{\omega} + 2\tilde{u}_j\zeta_j + \left(\zeta_j^2 - \frac{3}{2}\right)\tilde{\tau} - \tilde{\Phi}\right], \tag{50}$$

$$\tilde{\omega} = \int \tilde{\Phi}E(\boldsymbol{\zeta})d\boldsymbol{\zeta}, \tag{51a}$$

$$\tilde{u}_i = \int \zeta_i\tilde{\Phi}E(\boldsymbol{\zeta})d\boldsymbol{\zeta}, \tag{51b}$$

$$\tilde{\tau} = (2/3)\int (\zeta_j^2 - 3/2)\tilde{\Phi}E(\boldsymbol{\zeta})d\boldsymbol{\zeta}. \tag{51c}$$

Here, we note that the linearized equation of state holds, i.e.,

$$\tilde{P} = \tilde{\omega} + \tilde{\tau}. \tag{52}$$

The boundary condition on the cylinders is given by

$$\tilde{\Phi} = \tilde{\kappa}_w \quad \text{for } \zeta_j n_j > 0, \tag{53}$$

with

$$\tilde{\kappa}_w = -2\sqrt{\pi}\int_{\zeta_j n_j<0} \zeta_j n_j\tilde{\Phi}E(\boldsymbol{\zeta})d\boldsymbol{\zeta}, \tag{54}$$

where n_i $(n_3=0)$ is the unit normal vector to the cylinder surface pointed to the gas region.

Let us set the perturbed velocity distribution function $\tilde{\Phi}$ in the form

$$\tilde{\Phi} = C_P[y_1 + \Phi(y_1,y_2,\zeta_i)], \tag{55}$$

where Φ is periodic in y_i with period 1. Correspondingly, the macroscopic quantities are expressed as

$$\tilde{\omega} = C_P[y_1 + \omega(y_1,y_2)], \tag{56a}$$

$$\tilde{u}_i = C_P[u_i(y_1,y_2)], \tag{56b}$$

$$\tilde{\tau} = C_P[\tau(y_1,y_2)], \tag{56c}$$

$$\tilde{P} = C_P[y_1 + P(y_1,y_2)], \tag{56d}$$

where ω, u_i, τ, and P, which are also periodic in y_i with period 1, are defined in terms of Φ by Eqs. (51a)–(51c) and (52) without tilde $(\tilde{\ })$.

The equation and the boundary condition for Φ are as follows:

$$\zeta_1\frac{\partial\Phi}{\partial y_1} + \zeta_2\frac{\partial\Phi}{\partial y_2} = \frac{2}{\sqrt{\pi}}\frac{1}{\mathrm{Kn}}\left[\omega + 2u_j\zeta_j + \left(\zeta_j^2 - \frac{3}{2}\right)\tau - \Phi\right] - \zeta_1 \quad (\mathbf{y}\in Y_f), \tag{57}$$

$$\Phi = \kappa_w \quad \text{for } \zeta_j n_j > 0 \quad (\mathbf{y}\in S), \tag{58}$$

$$\kappa_w = -2\sqrt{\pi}\int_{\zeta_j n_j<0} \zeta_j n_j\Phi E(\boldsymbol{\zeta})d\boldsymbol{\zeta}, \tag{59}$$

$$\Phi\text{: periodic} \quad (y_1 = \pm 0.5, \quad y_2 = \pm 0.5), \tag{60}$$

where Y_f and S are defined by

$$Y_f = \{(y_1,y_2)|(y_1^2+y_2^2)^{1/2} \geqslant \hat{r}_c, \ \ |y_1| \leqslant 0.5, \ \ |y_2| \leqslant 0.5\},$$
$$S = \{(y_1,y_2)|(y_1^2+y_2^2)^{1/2} = \hat{r}_c\}, \tag{61}$$

with

$$\hat{r}_c = r_c/\ell \tag{62}$$

(see Fig. 2), and the range of $\mathbf{y}=(y_1,y_2)$ is restricted to Y_f with the periodic condition (60). Thus, the problem is reduced to solving the boundary-value problem (57)–(60) for a given set of parameters $(\hat{r}_c, \mathrm{Kn})$.

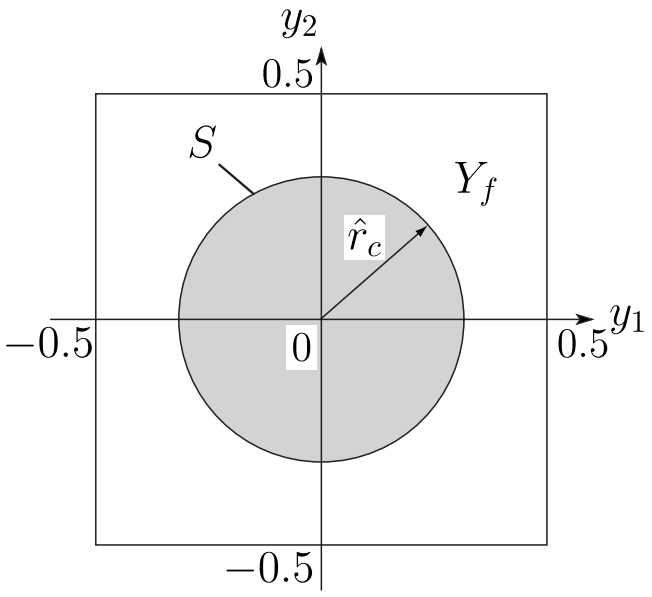

FIG. 2. The unit cell in the dimensionless (y_1, y_2) plane.

Our main interest here is to compute the mass-flow rate through a cross section $Y_1=$const (for unit width in the Y_3 direction) in the unit cell. If we denote such a mass-flow rate by $2C_P p_0 \ell (2RT_0)^{-1/2} M_P$, M_P is given by

$$M_P = \int_{-0.5}^{0.5} \left[\int \zeta_1 \Phi E(\boldsymbol{\zeta}) d\boldsymbol{\zeta} \right] dy_2 = \int_{-0.5}^{0.5} u_1 dy_2 \quad (y_1 = 0.5). \tag{63}$$

It should be noted that M_P is independent of y_1 and thus the cross section can be chosen arbitrarily. In our computation, we compute M_P at $y_1=0.5$.

Finally, let us remark that the solution Φ which is symmetric with respect to $y_2=0$ (the y_1 axis), i.e., $\Phi(y_1,-y_2,\zeta_1,-\zeta_2,\zeta_3)=\Phi(y_1,y_2,\zeta_1,\zeta_2,\zeta_3)$, and antisymmetric with respect to $y_1=0$ (the y_2 axis), i.e., $\Phi(-y_1,y_2,-\zeta_1,\zeta_2,\zeta_3)=-\Phi(y_1,y_2,\zeta_1,\zeta_2,\zeta_3)$, is compatible with the equation and the boundary conditions. Consequently, the macroscopic quantities and κ_w satisfy the following relations: $\mathfrak{h}(y_1,-y_2)=\mathfrak{h}(y_1,y_2)$ for $\mathfrak{h}=(\omega,\tau,P,u_1,\kappa_w)$, $u_2(y_1,-y_2)=-u_2(y_1,y_2)$, $\mathfrak{h}(-y_1,y_2)=-\mathfrak{h}(y_1,y_2)$ for $\mathfrak{h}=(\omega,\tau,P,u_2,\kappa_w)$, and $u_1(-y_1,y_2)=u_1(y_1,y_2)$. These relations are used to reduce the numerical expense.

B. Integral equations

One difficulty inherent in the numerical analysis of the present problem arises from the fact that the velocity distribution function contains generally discontinuities around a convex body.[59] In the present geometry, a discontinuity propagates from the surfaces of the cylinders along their tangential lines in the (y_1,y_2) plane. The discontinuity decays with distance from the boundary owing to molecular collisions and is appreciable over the distance of the order of the mean free path (or Kn). When Kn is small, the region where the discontinuity is appreciable is confined at the bottom of the Knudsen layer [the S layer[4,5,59] (see also Ref. 60)]. On the other hand, when Kn is not small, the discontinuity extends over the entire region of Y_f in the unit cell. Thus, the direct numerical analysis becomes very involved even for the present seemingly simple geometry. However, in the case of the linearized BGK collision operator under the diffuse reflection boundary condition, we can avoid this difficulty by transforming the system of equations into a system of linear integral equations for the macroscopic variables (i.e., ω, u_i, τ, and κ_w). Thus, an accurate numerical analysis becomes reachable. Therefore, in the present study, we will solve the integral equations derived from Eqs. (57)–(60). It may be noted that a finite difference method which is capable to capture the discontinuity in the velocity distribution function has been developed for some simple geometry and has been applied to fundamental problems (e.g., Refs. 59 and 61–66).

Now, let us derive the integral equations corresponding to Eqs. (57)–(60). To this end, we integrate Eq. (57) along its characteristics under the boundary condition (58), and substitute the result into Eqs. (51a)–(51c) (without tilde) and (59) to eliminate Φ. After carrying out the integration with respect to the molecular velocity ζ_i, we obtain a set of linear integral equations for ω, u_i, τ, and κ_w. In the following analysis, we introduce

$$k = (\sqrt{\pi}/2)\mathrm{Kn}, \tag{64}$$

and use k instead of Kn. Then, the resulting equations are summarized as follows:

$$\begin{pmatrix} \omega(\mathbf{y}) \\ u_i(\mathbf{y}) \\ (3/2)\tau(\mathbf{y}) \end{pmatrix} = \frac{1}{\pi k} \int_{D(\mathbf{y})} \frac{1}{|\mathbf{y}_* - \mathbf{y}|} \mathbb{K}(\mathbf{y},\mathbf{y}_*;k) \begin{pmatrix} \omega(\mathbf{y}_*) \\ u_j(\mathbf{y}_*) \\ \tau(\mathbf{y}_*) \end{pmatrix} d\mathbf{y}_* - \frac{1}{\pi} \int_{L(\mathbf{y})} \frac{\mathfrak{r}_j n_j(\mathbf{y}_*)}{|\mathbf{y}_* - \mathbf{y}|} \mathbb{K}_w(\mathbf{y},\mathbf{y}_*;k) \kappa_w(\mathbf{y}_*) dl(\mathbf{y}_*) + \begin{pmatrix} Ih_\omega \\ Ih_i \\ Ih_\tau \end{pmatrix} \quad (\mathbf{y} \in Y_f), \tag{65}$$

$$\kappa_w(\mathbf{y}) = \frac{2}{\pi^{1/2} k} \int_{D(\mathbf{y})} \frac{\mathfrak{r}_k n_k(\mathbf{y})}{|\mathbf{y}_* - \mathbf{y}|} \mathbb{W}(\mathbf{y},\mathbf{y}_*;k) \begin{pmatrix} \omega(\mathbf{y}_*) \\ u_j(\mathbf{y}_*) \\ \tau(\mathbf{y}_*) \end{pmatrix} d\mathbf{y}_* - \frac{2}{\pi^{1/2}} \int_{L(\mathbf{y})} \frac{\mathfrak{r}_j n_j(\mathbf{y}) \mathfrak{r}_k n_k(\mathbf{y}_*)}{|\mathbf{y}_* - \mathbf{y}|} J_2(|\mathbf{y}_* - \mathbf{y}|/k) \times \kappa_w(\mathbf{y}_*) dl(\mathbf{y}_*) + Ih_w \quad (\mathbf{y} \in S), \tag{66}$$

$$\omega(\mathbf{y} + \mathbf{e}_i) = \omega(\mathbf{y}), \quad u_i(\mathbf{y} + \mathbf{e}_i) = u_i(\mathbf{y}), \quad \tau(\mathbf{y} + \mathbf{e}_i) = \tau(\mathbf{y}), \quad \kappa_w(\mathbf{y} + \mathbf{e}_i) = \kappa_w(\mathbf{y}), \tag{67}$$

where $\mathbf{y}_*$ is the integration variable for $\mathbf{y}$, $d\mathbf{y}_* = dy_{*1} dy_{*2}$, $dl(\mathbf{y}_*)$ is the line element along the boundary at $\mathbf{y}_*$, $\mathfrak{r}_i = (y_{*i} - y_i)/|\mathbf{y}_* - \mathbf{y}|$, $\mathbf{e}_i$ is the unit vector pointing toward the y_i direction, $\mathbb{K}(\mathbf{y},\mathbf{y}_*;k)$, $\mathbb{K}_w(\mathbf{y},\mathbf{y}_*;k)$, and $\mathbb{W}(\mathbf{y},\mathbf{y}_*;k)$ are, respectively, the 4×4, 4×1, and 1×4 matrices given by

$$\mathbb{K} = \begin{pmatrix} J_0 & -2J_1\mathfrak{r}_1 & -2J_1\mathfrak{r}_2 & J_2 - J_0 \\ -J_1\mathfrak{r}_1 & 2J_2\mathfrak{r}_1^2 & 2J_2\mathfrak{r}_1\mathfrak{r}_2 & -(J_3 - J_1)\mathfrak{r}_1 \\ -J_1\mathfrak{r}_2 & 2J_2\mathfrak{r}_1\mathfrak{r}_2 & 2J_2\mathfrak{r}_2^2 & -(J_3 - J_1)\mathfrak{r}_2 \\ J_2 - J_0 & -2(J_3 - J_1)\mathfrak{r}_1 & -2(J_3 - J_1)\mathfrak{r}_2 & J_4 - 2J_2 + (3/2)J_0 \end{pmatrix}, \tag{68a}$$

$$\mathbb{K}_w = \begin{pmatrix} J_1 \\ -J_2\mathfrak{r}_1 \\ -J_2\mathfrak{r}_2 \\ J_3 - J_1 \end{pmatrix}, \tag{68b}$$

$$\mathbb{W} = (J_1, -2J_2\mathfrak{r}_1, -2J_2\mathfrak{r}_2, J_3 - J_1), \tag{68c}$$

and the inhomogeneous terms $(Ih_\omega, Ih_i, Ih_\tau, Ih_w)$ are given by

$$\begin{pmatrix} Ih_\omega \\ Ih_i \\ Ih_\tau \end{pmatrix} = \frac{k}{\pi}\int_{L(\mathbf{y})} \mathfrak{r}_1 \frac{\mathfrak{r}_j n_j(\mathbf{y}_*)}{|\mathbf{y}_* - \mathbf{y}|} \begin{pmatrix} J_2 \\ -J_3\mathfrak{r}_i \\ J_4 - J_2 \end{pmatrix} dl(\mathbf{y}_*) - \begin{pmatrix} 0 \\ (k/2)\delta_{i1} \\ 0 \end{pmatrix}, \tag{69a}$$

$$Ih_w = \frac{2k}{\pi^{1/2}}\int_{L(\mathbf{y})} \mathfrak{r}_1 \frac{\mathfrak{r}_j n_j(\mathbf{y})\mathfrak{r}_k n_k(\mathbf{y}_*)}{|\mathbf{y}_* - \mathbf{y}|} J_3 dl(\mathbf{y}_*) + \frac{\pi^{1/2}}{2} k n_1 \tag{69b}$$

(δ_{ij} is the Kronecker delta). J_n is the Abramowitz function[67] defined by

$$J_n(x) = \int_0^\infty \zeta^n \exp\left(-\zeta^2 - \frac{x}{\zeta}\right) d\zeta. \tag{70}$$

The arguments of J_n in Eqs. (68) and (69) are commonly $|\mathbf{y}_* - \mathbf{y}|/k$. The domain of area integration $D(\mathbf{y})$ is the region occupied by the gas visible from $\mathbf{y}$ in the (y_1, y_2) plane, and that of the line integration $L(\mathbf{y})$ is the surfaces of the cylinders visible from $\mathbf{y}$ in the (y_1, y_2) plane (see Fig. 3). In carrying out the integrations, the periodic condition (67) should be applied when the variable $\mathbf{y}_*$ is outside Y_f. The details of the derivation of these integral equations can be found in Ref. 5. Equations (65) and (66) are advantageous because the velocity distribution function has been eliminated from the equations. The numerical difficulty associated with the discontinuity in the velocity distribution function is now reduced to the level of numerical integrations in a complex domain which varies with the point $\mathbf{y}$.

Equations (65)–(67) can be solved by the method of successive approximation. The actual computation is carried out following Ref. 68, where the same type of integral equations has been solved to investigate a rarefied gas flow between two noncoaxial circular cylinders maintained at two different uniform temperatures. We only mention that a spatially fixed rectangular grid system was used for the variable $\mathbf{y}$ (the specific choice of this grid will be given in Sec. III C below), and an overlapped plane polar grid system with its origin at $\mathbf{y}$ was used for the variable $\mathbf{y}_*$ to carry out the area and line integrations, where the values needed for numerical integrations are obtained from those associated with the rectangular grid system by interpolation.

It should be also noted that, in the present problem, $|\mathbf{y}_* - \mathbf{y}|$ can be arbitrarily large for a given $\mathbf{y}$, and therefore, we have to restrict the domain of integration to a finite domain in order to perform numerical integrations. Since the Abramowitz function $J_n(x)$ is a rapidly decaying function, this is safely done by choosing a sufficiently large number R_D such that the integrands are negligibly small for $|\mathbf{y}_* - \mathbf{y}| > R_D$. More precisely, if we denote by $D_R(\mathbf{y})$ the circular domain centered at $\mathbf{y}$ with a radius R_D in the (y_{*1}, y_{*2}) plane, the actual area (line) integrals in Eqs. (65) and (66) are carried out in $D(\mathbf{y}) \cap D_R(\mathbf{y})$ $[L(\mathbf{y}) \cap D_R(\mathbf{y})]$. In the actual computation, we set $R_D = kr_D$ and specify r_D rather than R_D. The value of r_D used in our numerical computations is 21.8 for

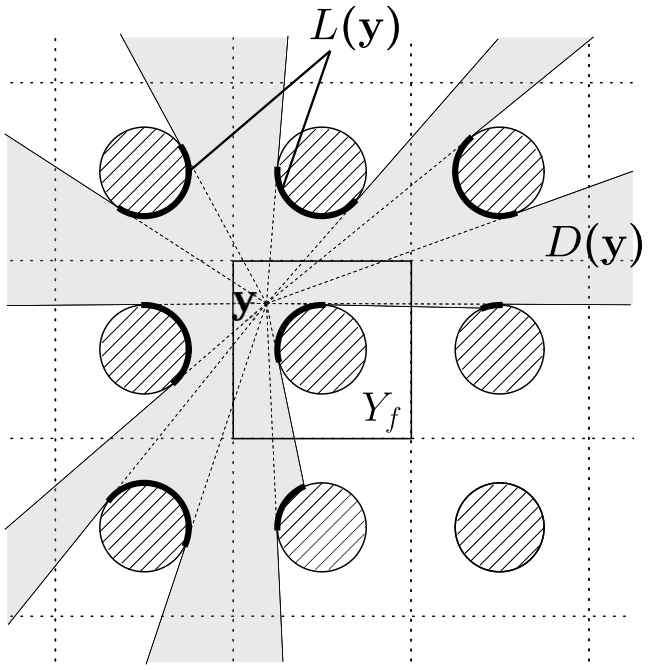

FIG. 3. The domain of integration. $D(\mathbf{y})$ is the region occupied by the gas visible from $\mathbf{y}$, whereas $L(\mathbf{y})$ is the surfaces of the cylinders visible from $\mathbf{y}$.

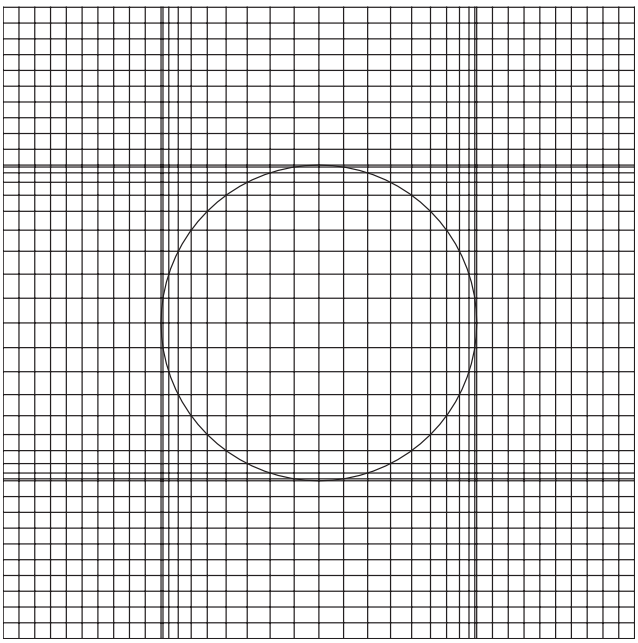

FIG. 4. Rectangular grid system in the unit cell fixed in space. System (I) for $\hat{r}_c=0.25$. A circle with the radius $\hat{r}_c$ is shown to indicate the cylinder surface.

$0.1 \leqslant k \leqslant 0.15$, 16.7 for $k=0.2$, 12.0 for $0.3 \leqslant k \leqslant 0.7$, and 7.9 for $0.8 \leqslant k \leqslant 5$. We refer to Ref. 68 for the further details of the numerical computation, where the detailed description of the numerical method can be found.

C. Rectangular grid system fixed in space

First, we approximate the cylinder by a regular polygon with $4\hat{K}$ sides, where the vertices are the intersections of the cylinder surface and the $4\hat{K}$ radial lines emitted isotropically from the center of the cylinder. Then, the domain $|y_1| \leqslant 0.5$ and $|y_2| \leqslant 0.5$ is divided by $(2M+1)$ parallel lines perpendicular to the y_1 axis and by $(2N+1)$ parallel lines perpendicular to the y_2 axis. The $(2M+1)$ [or $(2N+1)$] lines are composed of $(2\hat{K}+1)$ lines passing through the vertices of the polygon in the interval $|y_1| \leqslant \hat{r}_c$ (or $|y_2| \leqslant \hat{r}_c$) and $2(M-\hat{K})$ [or $2(N-\hat{K})$] uniformly spaced lines in the interval $\hat{r}_c < |y_1| \leqslant 0.5$ (or $\hat{r}_c < |y_2| \leqslant 0.5$).

In the present computation, we used three different sizes of the rectangular grid system for accuracy and comparison: (I) $M=N=20$, $\hat{K}=10$; (II) $M=N=40$, $\hat{K}=20$; and (III) $M=N=80$, $\hat{K}=40$ (see Fig. 4).

D. Asymptotic analysis for small *k*

Before presenting numerical results, in this subsection, we return to the original system (57)–(60) and discuss the solution for small k (or Kn). When k is small, the mean free path of the gas is small compared to the cell size, and the flow field in the unit cell is expected to be described by the macroscopic variables via fluid-dynamic equations. A general theory describing flows of slightly rarefied gases (asymptotic theory for small Knudsen numbers) has been developed by Sone and co-workers[4,5,69–74] for a wide class of problems. Thus, we can make use of this theory to investigate the present problem for small k.

According to the theory,[4,5] the solution Φ can be written in the following form:

$$\Phi = \Phi_G + \Phi_K, \tag{71}$$

where Φ_G is the moderately varying overall solution (the Grad–Hilbert solution) and Φ_K is the Knudsen-layer correction to Φ_G only appreciable in a thin layer (the Knudsen layer) adjacent to the boundary whose length scale of variation is of the order of k (or of the mean free path) in the direction normal to the boundary. Φ_G and Φ_K are expanded in k as follows:

$$\Phi_G = \frac{1}{k}(\phi_{G(0)} + \phi_{G(1)}k + \phi_{G(2)}k^2 + \cdots), \tag{72a}$$

$$\Phi_K = \frac{1}{k}(\phi_{K(1)}k + \phi_{K(2)}k^2 + \cdots). \tag{72b}$$

Correspondingly, the macroscopic quantities $\mathfrak{h}$ ($\mathfrak{h}=\omega$, u_i, τ, or P) are also expanded as

$$\mathfrak{h} = \mathfrak{h}_G + \mathfrak{h}_K, \tag{73a}$$

$$\mathfrak{h}_G = \frac{1}{k}(\mathfrak{h}_{G(0)} + \mathfrak{h}_{G(1)}k + \mathfrak{h}_{G(2)}k^2 + \cdots), \tag{73b}$$

$$\mathfrak{h}_K = \frac{1}{k}(\mathfrak{h}_{K(1)}k + \mathfrak{h}_{K(2)}k^2 + \cdots), \tag{73c}$$

where $\mathfrak{h}_G$ is the Grad–Hilbert part of $\mathfrak{h}$ corresponding to Φ_G and $\mathfrak{h}_K$ is its Knudsen-layer correction corresponding to Φ_K. The expansion coefficients $\mathfrak{h}_{G(m)}$ of the Grad–Hilbert part are subject to the Stokes set of equations.[4,5] Here, we only give the explicit equations which determine the flow velocity $u_{iG(m)}$ for conciseness. That is, the equations are given by

$$\frac{\partial u_{iG(m)}}{\partial y_i} = 0, \tag{74a}$$

$$\frac{\partial P_{G(m+1)}}{\partial y_i} - \frac{\partial^2 u_{iG(m)}}{\partial y_j^2} = -\delta_{i1}\delta_{m0} \tag{74b}$$

$(m=0,1,2,\ldots)$. The corresponding boundary conditions on the surface of the cylinder (i.e., $r=\hat{r}_c$ with $r=|\mathbf{y}|$) up to $m=1$ are given by

$$u_{rG(0)} = u_{\theta G(0)} = 0, \tag{75}$$

for $m=0$ and

$$u_{rG(1)} = 0, \tag{76a}$$

$$u_{\theta G(1)} = -k_0 \frac{\partial u_{\theta G(0)}}{\partial r}, \tag{76b}$$

for $m=1$, where $u_{rG(m)}$ and $u_{\theta G(m)}$ are the radial and circumferential components of $u_{iG(m)}$, respectively. The numerical

value of the slip coefficient k_0 for the BGK equation under the diffuse reflection condition is given by[4,5]

$$k_0 = -1.016\,19. \tag{77}$$

The above system of equations should be supplemented by the periodic condition on $\partial Y_f \cap \partial Y$.

The leading order flow velocity $u_{iG(0)}$ is determined together with $P_{G(1)}$ as the solution of the Stokes set of equations (74a) and (74b) (with $m=0$) under the nonslip boundary condition (75), and the next order flow velocity $u_{iG(1)}$ is determined together with $P_{G(2)}$ as the solution of the Stokes set of equations (74a) and (74b) (with $m=1$) under the slip boundary conditions (76a) and (76b). Moreover, if we set $(u_{iG(1)}, P_{G(2)}) = k_0(\hat{u}_{iG(1)}, \hat{P}_{G(2)})$, we can get rid of k_0 from the equations. In the present study, these Stokes equations were numerically solved by a finite difference method to obtain $u_{iG(0)}$ and $\hat{u}_{iG(1)}$.

Once we obtain $u_{iG(0)}$ and $\hat{u}_{iG(1)}$, we can readily compute the approximate value of M_P for small k (or Kn). That is, if we write M_P as

$$M_P = \frac{1}{k} M_{P(0)} + k_0 \hat{M}_{P(1)} + O(k), \tag{78}$$

the coefficients $M_{P(0)}$ and $\hat{M}_{P(1)}$ are given by

$$\begin{bmatrix} M_{P(0)} \\ \hat{M}_{P(1)} \end{bmatrix} = \int_{-0.5}^{0.5} \begin{bmatrix} u_{1G(0)} \\ \hat{u}_{1G(1)} \end{bmatrix} dy_2 \quad (y_1 = 0.5). \tag{79}$$

Here, we have taken into account the fact that the Knudsen-layer correction $u_{1K(1)}$ is appreciable only in the Knudsen layer adjacent to the boundary with the thickness of the order of k. $M_{P(0)}$ and $\hat{M}_{P(1)}$ depend only on $\hat{r}_c$ (i.e., geometry) and their numerical values are obtained as $(M_{P(0)}, \hat{M}_{P(1)}) = (-0.019\,90, 0.2154)$ for $\hat{r}_c = 0.25$ and $(M_{P(0)}, \hat{M}_{P(1)}) = (-0.010\,98, 0.1447)$ for $\hat{r}_c = 0.3$. The result for M_P based on the asymptotic expression (78) is also included in the numerical results given in the following subsection. Incidentally, the coefficients $M_{P(0)}$ and $k_0 \hat{M}_{P(1)}$ are directly related to the permeability constant and the Klinkenberg factor appearing in the Klinkenberg's law[75] describing the effective permeability of the low pressure gas flow through a porous medium. The relation to the Klinkenberg's law is given in Appendix A.

E. Numerical results

In this section, we show some numerical results. The computations were made for two different diameters of the cylinders, i.e., $\hat{r}_c = 0.25$ and 0.3, and for various Kn ranging from 0.1 to 5. The results presented in the following are based on the grid system (II) (see Sec. III C) except those in Table I. In Fig. 5, we show M_P versus k for $\hat{r}_c = 0.25$ and 0.3. Table I shows the numerical values of M_P, where the comparison of the results for the three grid systems is made. In the figure, numerical values of M_P based on the direct numerical solutions of the integral equations are shown by the symbols. $-M_P$ first decreases with k and then increases. $-M_P$ takes its minimum value at an intermediate value of k (around $k=0.9$ for $\hat{r}_c = 0.25$ and around $k=0.8$ for $\hat{r}_c = 0.3$). This corresponds to the Knudsen minimum, which has been known for rarefied gas flows through a channel or a pipe. The present result confirms the existence of the minimum in the case of the in-line array of circular cylinders. $-M_P$ takes

TABLE I. M_P vs k for $\hat{r}_c = 0.25$ and 0.3. Comparison of the results for three grid systems (cf. Sec. III C).

	$-M_P$					
	$\hat{r}_c = 0.25$			$\hat{r}_c = 0.3$		
k	(I)	(II)	(III)	(I)	(II)	(III)
0.1	0.4195	0.4191		0.2582	0.2579	
0.15	0.3554	0.3550		0.2221	0.2218	
0.2	0.3243	0.3238		0.2045	0.2041	
0.3	0.2945	0.2940		0.1876	0.1871	
0.4	0.2810	0.2804		0.1802	0.1796	
0.5	0.2739	0.2733	0.2731	0.1764	0.1759	0.1757
0.6	0.2700	0.2694		0.1746	0.1740	
0.8	0.2667	0.2660		0.1735	0.1728	
1	0.2669	0.2661	0.2659	0.1742	0.1735	0.1734
1.2	0.2684	0.2676	0.2674	0.1757	0.1750	0.1749
1.4	0.2706	0.2698		0.1775	0.1768	
1.6	0.2732	0.2724		0.1794	0.1788	
1.8	0.2760	0.2752		0.1815	0.1808	
2	0.2789	0.2780	0.2778	0.1834	0.1828	0.1826
3	0.2931	0.2921		0.1929	0.1922	
4	0.3059	0.3048		0.2011	0.2004	
5	0.3171	0.3160		0.2080	0.2074	

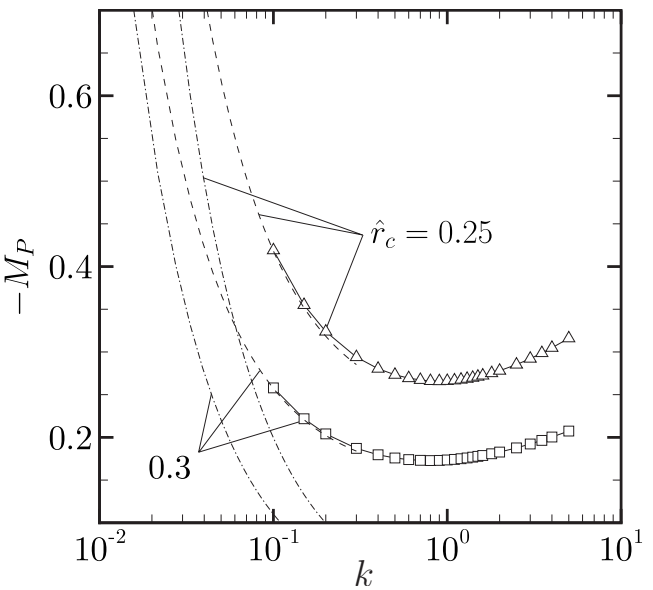

FIG. 5. M_P vs k for $\hat{r}_c = 0.25$ and 0.3. M_P based on the direct numerical solutions of the integral equations is shown by the symbols which are connected with solid lines. M_P based on the asymptotic expression up to the order of k^0 [i.e., the first two terms of Eq. (78)] is shown by the dashed lines. For comparison, M_P based on the solution of the Stokes equations with nonslip boundary condition [i.e., the first term of Eq. (78)] is also shown by the dot-dashed lines.

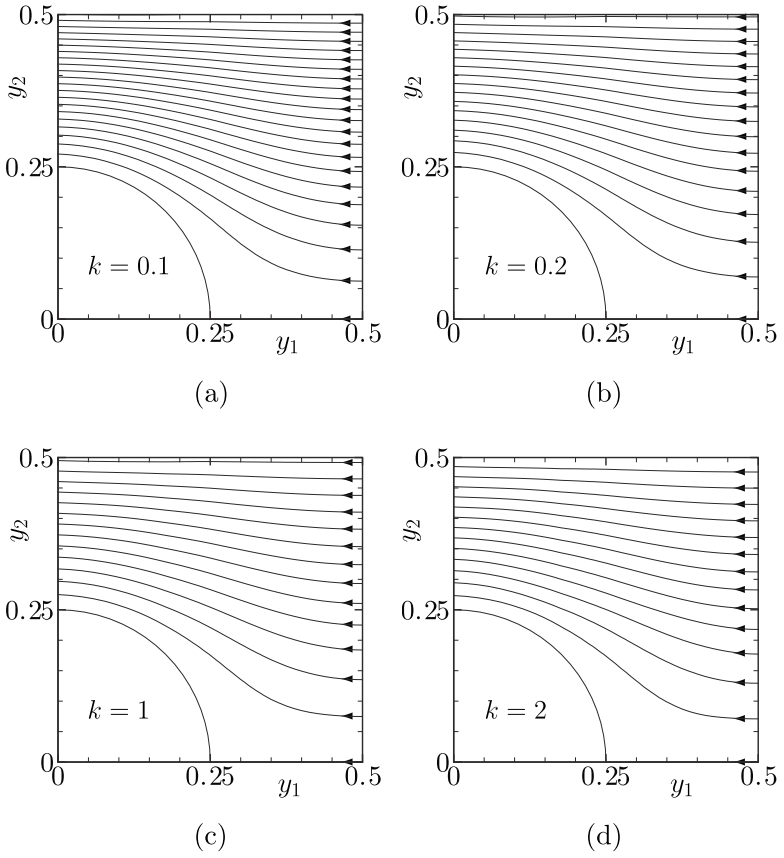

FIG. 6. Streamlines of the flow in the case $\hat{r}_c=0.25$: (a) $k=0.1$, (b) $k=0.2$, (c) $k=1$, and (d) $k=2$. The lines indicate the isolines of the stream function $\psi=-0.01n$ $(n=0,1,\ldots)$ defined by $u_1=\partial\psi/\partial y_2$ and $u_2=-\partial\psi/\partial y_1$. $\psi=0$ $(n=0)$ on the y_1 axis and ψ (n) decreases (increases) monotonically with the distance from the y_1 axis. The arrows indicate the direction of the flow.

larger values for smaller $\hat{r}_c$. In the figure, we also included M_P based on the asymptotic solutions up to the order of k^0 [i.e., the first two terms of Eq. (78)] as well as M_P based on the asymptotic solutions up to the order of k^{-1} [i.e., the first term of Eq. (78)]. The former takes into account the velocity slip on the boundary due to the gas-rarefaction effect, whereas the latter does not. Compared to the latter, the former (the asymptotic solutions up to the order k^0) agrees well with the direct numerical solutions. The discrepancy of the asymptotic solutions from the direct solutions is less than 0.5% at $k=0.1$ for both values of $\hat{r}_c$. The asymptotic approach seems to provide a useful alternative to the direct numerical solution for small k $(k<0.2)$.

In Fig. 6, we show the streamlines of the flow obtained by the direct numerical analysis of the integral equations in the case $\hat{r}_c=0.25$ for various k, i.e., $k=0.1$, 0.2, 1, and 2. In Fig. 7, we compare the streamlines for $k=0.1$ and those for $k=1$ for the same value of $\hat{r}_c$. The streamlines of the Stokes flow, i.e., the solution of Eqs. (74a) and (74b) (with $m=0$) under the nonslip boundary condition (75), are also shown in Fig. 7 for comparison. The streamlines for $k=0.1$ and those for $k=1$ are rather close except in the regions above and in front of the cylinder. Both of those exhibit significant deviations from the streamlines of the Stokes flow near the surface of the cylinder.

F. Comment on numerical data

Here, we make brief comments on the accuracy of the numerical data. We verified that the values of r_D (see Sec. III B) used in the numerical computations are sufficiently large by confirming that the values of M_P shown in Table I do not undergo significant changes by the increase in r_D for some typical cases of k using the grid system (I). The observed difference was at most 2 in the last figure in the case of $\hat{r}_c=0.25$ and at most 1 in the last figure in the case of $\hat{r}_c$

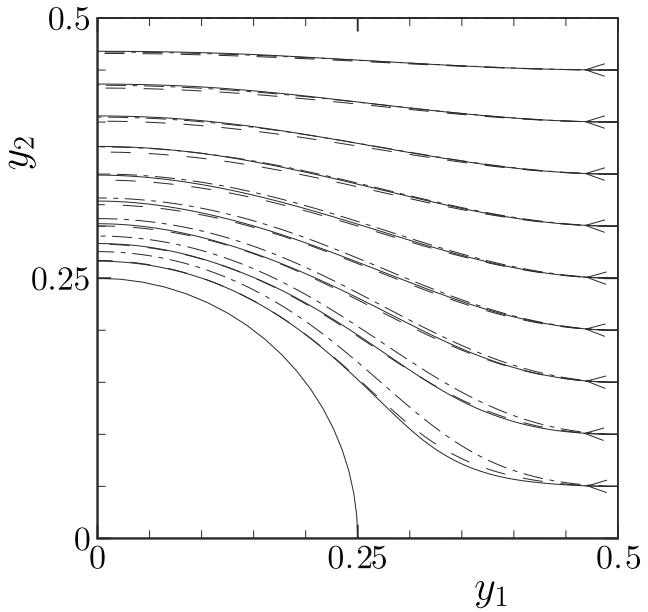

FIG. 7. Comparison between the streamlines for $k=0.1$ and those for $k=1$ $(\hat{r}_c=0.25)$. The streamlines for $k=0.1$ are shown by solid lines, whereas those for $k=1$ are shown by dashed lines. For comparison, the streamlines based on the solution of the Stokes equation under the nonslip boundary condition are shown by dot-dashed lines. The arrows indicate the direction of the flow.

=0.3. Here, we have increased r_D from (21.8, 16.7, 12.0, 7.9) to (27.1, 21.8, 16.7, 12.0) depending on the value of k.

Because of the conservation of mass, M_P should be independent of y_1. We computed M_P at every grid line y_1 =const and confirmed that the mass conservation is satisfied with sufficient accuracy. For the grid system (II), the variation is less than 0.21% in the case of $\hat{r}_c=0.25$ and less than 0.25% in the case of $\hat{r}_c=0.3$.

G. Diffusion coefficient of the fluid model

We conclude this section by deriving the diffusion tensor $\mathbf{M}_P$ in Eq. (48b) for the in-line array of circular cylinders. Here, the fluid model (48a)–(48c) is considered to be two-dimensional (i.e., $\partial_{x_3}=0$) and $\mathbf{M}_P$ should be interpreted as a 2×2 matrix. We first note the following correspondence between the two-dimensional version of the cell auxiliary problem (33)–(37) (with $\partial_{y_3}=0$) and the boundary-value problem considered in this section, i.e., Eqs. (57)–(60): the quantities $(\Phi,\omega,u_i,\tau,P,\kappa_w,\mathrm{Kn})$ in this section correspond to the quantities $(\Phi^1,\omega^1,u_i^1,\tau^1,P^1,\kappa_w^1,K_0)$ in Sec. II [the subsidiary condition (37) is satisfied by Φ]. Consequently, the mass-flow rate M_P in this section corresponds to M_{P11} in Sec. II. Since $\mathbf{M}_P$ is isotropic ($M_{P11}=M_{P22}$ and $M_{P12}=M_{P21}=0$) and since M_P has been obtained as a function of $k[=(\sqrt{\pi}/2)\mathrm{Kn}]$, the diffusion tensor $\mathbf{M}_P$ is expressed as

$$\mathbf{M}_P = M_P\left(\frac{\sqrt{\pi}}{2}K_0\right)\mathbf{I}, \tag{80}$$

where $\mathbf{I}$ is the 2×2 identity matrix.

Since we have obtained the diffusion tensor (or coefficient M_P), we can now apply the fluid model (48a)–(48c) [with Eq. (80)] to investigate isothermal flows through a porous medium consisting of an in-line array of cylinders induced by the pressure gradient (or difference). A simple example of such a flow will be given in the next section. Incidentally, the diffusion coefficient M_P is likely to diverge in the free molecular limit $K_0\to\infty$. This is attributed to the molecules which come from the infinity without undergoing any collision with the cylinders. If the cylinders are arranged in a staggered way, making the radius of the cylinders sufficiently large, the diffusion coefficient remains finite in the free molecular limit.[58]

IV. APPLICATION

In this section, we present an application of the fluid model to an isothermal pressure-driven flow through a porous medium. That is, we consider a porous slab made of an in-line array of circular cylinders, as shown in Fig. 8. The dimensions of the porous slab are L in the X_1 direction and infinitely long in the X_2 and X_3 directions, where X_i is the space rectangular coordinates. As before, the linear dimension of the unit cell is denoted by ℓ and the radius of the cylinder is denoted by r_c ($r_c/\ell<0.5$). The pressures of the gas at the two ends $X_1=0$ and L are kept at p_0 and p_1, respectively, while the temperatures (at both ends) are kept at an equal temperature T_0. The temperature of the cylinders (or that of the porous slab) is also kept at T_0. When $p_1>p_0$, a

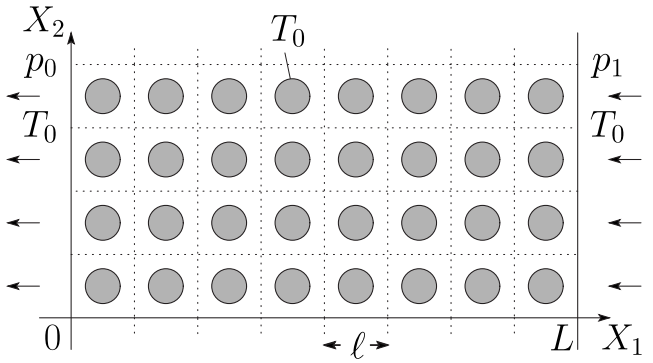

FIG. 8. A rarefied gas flow through a porous slab made of an in-line array of cylinders induced by the pressure difference.

flow is induced in the slab in the negative X_1 direction due to the pressure difference. We investigate the steady behavior of the flow on the basis of the BGK model by assuming that the molecular reflection on the solid boundary is diffusive.

Let us take L and p_0 as the reference length and the reference pressure, respectively, i.e., $p_*=p_0$. The present problem is characterized by the parameters

$$\epsilon=\frac{\ell}{L},\quad K_*=\frac{\ell_*}{\ell},\quad \hat{r}_c=\frac{r_c}{\ell},\quad \hat{p}_1=\frac{p_1}{p_0}, \tag{81}$$

where ℓ_* is the mean free path of the gas in the equilibrium state at rest with temperature T_0 and pressure p_0 (or density $\rho_0=p_0/RT_0$). In this section, we use the dimensional pressure p, density ρ, and flow velocity $\mathbf{v}$ (or v_i) in addition to their dimensionless counterparts. When ϵ is small, we can apply the fluid model (48a)–(48c) to describe the dimensionless pressure $\hat{p}(=p/p_0)$ [or the dimensionless density $\hat{\rho}(=\rho/\rho_0=\hat{p})$]. Thus, $\hat{p}$ is governed by the following equation:

$$\frac{d}{dx_1}M_1=0, \tag{82a}$$

$$M_1=M_P\left(\frac{\sqrt{\pi}}{2}K_0\right)\frac{d\hat{p}}{dx_1}, \tag{82b}$$

$$K_0=\frac{K_*}{\hat{p}}, \tag{82c}$$

where the subscript "(0)" which indicates the leading order quantity in ϵ is omitted. It should be noted that M_P depends also on $\hat{r}_c$. The above equations (82a)–(82c) will be solved under the following boundary conditions:

$$\hat{p}=1\quad (x_1=0),$$
$$\hat{p}=\hat{p}_1=p_1/p_0\quad (x_1=1). \tag{83}$$

The mass-flow rate $\tilde{M}$ in the X_1 direction through the unit cell (for unit width in the X_3 direction) is given by

$$\tilde{M}/\ell\rho_0(2RT_0)^{1/2}=\epsilon M_1+O(\epsilon^2). \tag{84}$$

From Eqs. (82a)–(82c) and (83), the dimensionless mass-flow rate M_1 is simply expressed as

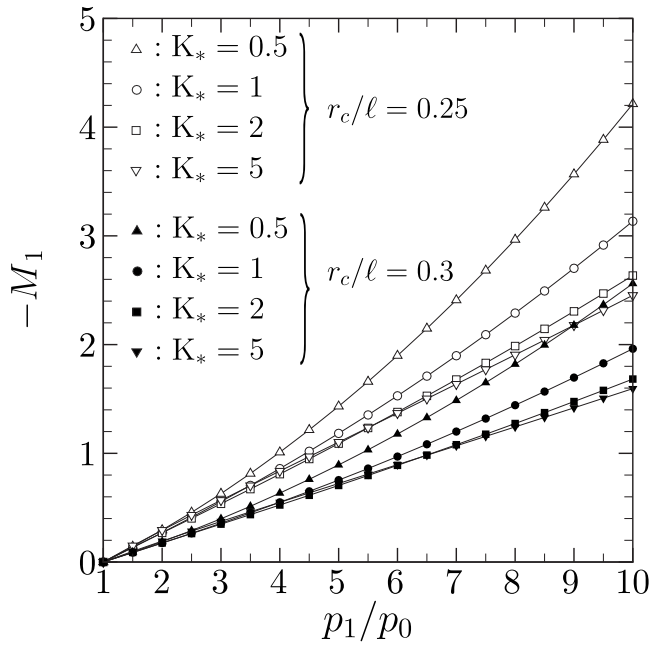

FIG. 9. M_1 vs p_1/p_0 for various K_* for $r_c/\ell=0.25$ and 0.3. The numerical results are shown by the symbols which are connected by the solid lines.

$$M_1 = \int_1^{\hat{p}_1} M_P\left(\frac{\sqrt{\pi}}{2}\frac{K_*}{\hat{p}}\right)d\hat{p}. \tag{85}$$

Once M_1 is determined from the above integral, the pressure profile is obtained from

$$x_1 = \frac{1}{M_1}\int_1^{\hat{p}} M_P\left(\frac{\sqrt{\pi}}{2}\frac{K_*}{t}\right)dt. \tag{86}$$

The integrals in Eqs. (85) and (86) are evaluated numerically with the aid of the numerical data for the diffusion coefficient M_P obtained in the previous section (Fig. 5 and Table I). More precisely, we have interpolated the numerical data obtained by the direct numerical analysis of the integral equations for $0.1\leqslant k\leqslant 5$, and used the asymptotic formula (78) for $k<0.1$, where $k=(\sqrt{\pi}/2)K_0$. The results are presented in Figs. 9–11. In Fig. 9, we show the dimensionless mass-flow rate M_1 versus $\hat{p}_1$ for various values of K_* and for $\hat{r}_c=0.25$ and 0.3. For a fixed K_*, $-M_1$ increases with the pressure ratio $\hat{p}_1$ and decreases with the radius of the cylinder $\hat{r}_c$. The curves for $K_*=0.5$ and 1 are convex with respect to $\hat{p}_1$ for the entire range of $\hat{p}_1$ shown in the figure for both $\hat{r}_c=0.25$ and 0.3. However, though it is rather hard to see it from the figure, the curves for $K_*=2$ and 5 are concave with respect to $\hat{p}_1$ up to a certain value of $\hat{p}_1$, and then they become convex for larger $\hat{p}_1$. The curves for $K_*=5$ take larger values of $-M_1$ than those for $K_*=2$ in the range $0<\hat{p}_1\lesssim 5.5$. This result will be explained in the following paragraphs.

To simplify the following calculation, we introduce a new function $\tilde{M}_P(K_0)=M_P(\sqrt{\pi}K_0/2)$ and use $\tilde{M}_P$ rather than M_P. If we differentiate Eq. (85) with respect to $\hat{p}_1$ twice, we obtain

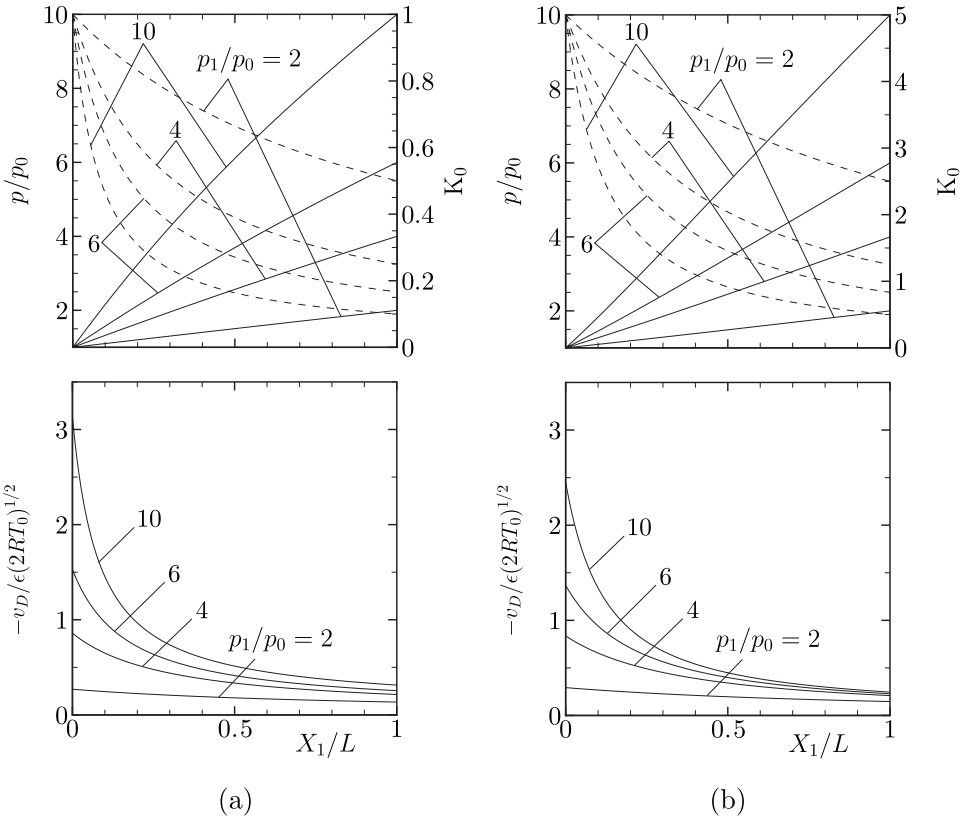

FIG. 10. Profiles of the pressure p, the local Knudsen number K_0, and the filter velocity v_D for various p_1/p_0 in the case of $r_c/\ell=0.25$: (a) $K_*=1$ and (b) $K_*=5$. In the upper panels, the profiles of the pressure are shown by solid lines and those of the local Knudsen number by dashed lines.

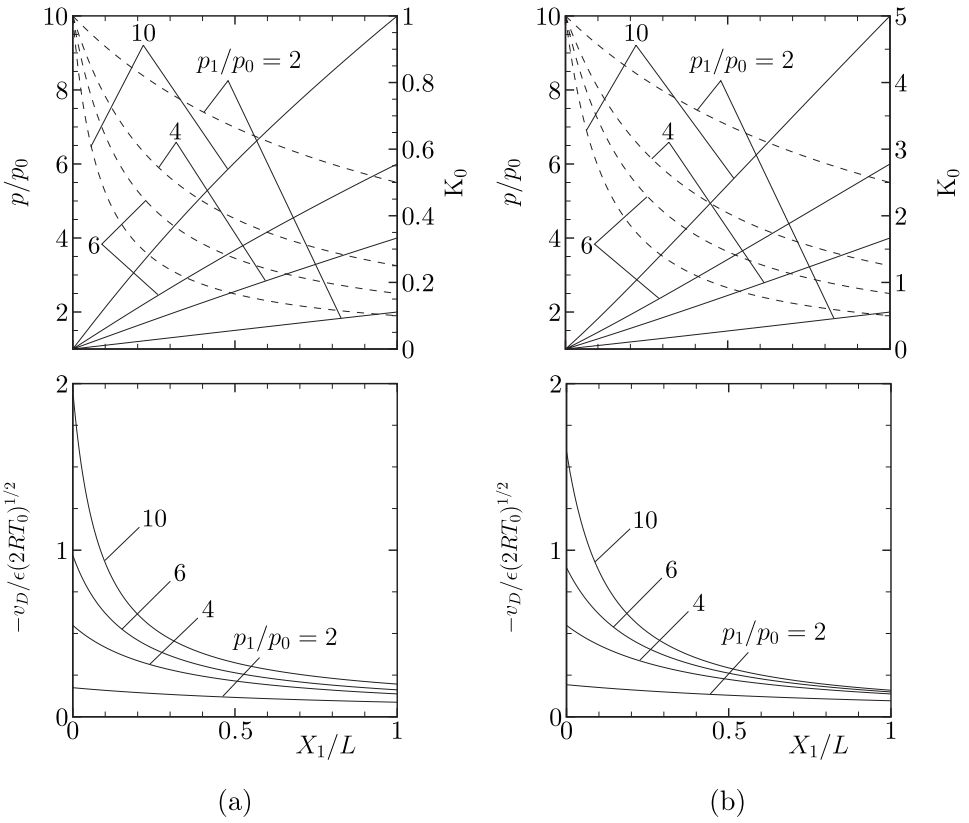

FIG. 11. Profiles of the pressure p, the local Knudsen number K_0, and the filter velocity v_D for various p_1/p_0 in the case of $r_c/\ell=0.3$: (a) $K_*=1$ and (b) $K_*=5$. See caption of Fig. 10.

$$\frac{d^2M_1}{d\hat{p}_1^2} = -\tilde{M}_P'\left(K_0 = \frac{K_*}{\hat{p}_1}\right)\frac{K_*}{\hat{p}_1^2}, \tag{87}$$

where $\tilde{M}_P'$ denotes the derivative of $\tilde{M}_P$ with respect to K_0. Let us denote by K_m the stationary point of $\tilde{M}_P$, i.e., $\tilde{M}_P'(K_m)=0$. That is, K_m corresponds to the value of the local Knudsen number at which the Knudsen minimum occurs and $-\tilde{M}_P'$ changes its sign from minus to plus across $K_0=K_m$ (cf. Fig. 5). In the following discussion, we also assume that $-\tilde{M}_P'$ remains positive for all $K_0>K_m$.

The above-mentioned result for the functional form of M_1 can be easily explained from Eq. (87) and from the fact that $K_*/\hat{p}_1$, at which $\tilde{M}_P'$ is evaluated in Eq. (87), is a decreasing function of $\hat{p}_1$. That is, when $K_*\leqslant K_m$, $K_*/\hat{p}_1$ remains less than K_m for the entire range of $\hat{p}_1>1$. For these values of $K_*/\hat{p}_1$, $-\tilde{M}_P'$ in Eq. (87) is always negative, and therefore $-M_1$ is a convex function of $\hat{p}_1$. On the other hand, when $K_*>K_m$, there exists a $\hat{p}_1(>1)$ such that $K_*/\hat{p}_1=K_m$ holds. We denote this value of $\hat{p}_1$ by $\hat{p}_c$, i.e., $\hat{p}_c=K_*/K_m$. Then, in the interval $1<\hat{p}_1<\hat{p}_c$, where $K_*/\hat{p}_1>K_m$, $-\tilde{M}_P'$ is positive, whereas in the interval $\hat{p}_1>\hat{p}_c$, where $K_*/\hat{p}_1<K_m$, $-\tilde{M}_P'$ is negative. Thus, it follows from Eq. (87) that $-M_1$ is concave for $1<\hat{p}_1<\hat{p}_c$ and convex for $\hat{p}_1>\hat{p}_c$; the point $\hat{p}_1=\hat{p}_c$ gives the point of inflection for a given $\hat{r}_c$.

As seen from the first equation of Eq. (25), the dimensionless flow velocity $\hat{\mathbf{v}}=(\hat{v}_1,\hat{v}_2,0)$ $[\hat{v}_i=v_i/(2RT_0)^{1/2}]$ is a small quantity of the order of ϵ. If we define the so-called filter velocity v_D (in the X_1 direction) by $v_D=\tilde{M}/\rho\ell$, it is given by

$$v_D/(2RT_0)^{1/2} = \epsilon M_1/\hat{p} + O(\epsilon^2). \tag{88}$$

In Figs. 10 and 11, we show the profiles of the pressure p, the local Knudsen number K_0, and the filter velocity v_D [based on the first term of Eq. (88)] for $K_*=1$ and 5 in the case $\hat{r}_c=0.25$ (Fig. 10) and $\hat{r}_c=0.3$ (Fig. 11). The pressure $\hat{p}$ increases monotonically in x_1 and, correspondingly, the local Knudsen number K_0 decreases. The flow speed becomes faster as we proceed downstream from $x_1=1$ $(X_1=L)$ to $x_1=0$ $(X_1=0)$.

From the functional form of $\tilde{M}_P(K_0)$, we can easily show that the profile (or the curvature) of the pressure $\hat{p}$ can be classified into the following three types: for a given $\hat{r}_c$, (i) when $K_*\leqslant K_m$, $\hat{p}(x_1)$ is concave; (ii) when $K_m<K_*<K_m\hat{p}_1$, there exists an x_c $(0<x_c<1)$ such that $\hat{p}(x_c)=K_*/K_m$, and $\hat{p}(x_1)$ is convex in the range $0\leqslant x_1<x_c$ and is concave in the range $x_c<x_1\leqslant 1$ (i.e., $x_1=x_c$ is the inflection point); (iii) when $K_*\geqslant K_m\hat{p}_1$, $\hat{p}(x_1)$ is convex. Here, K_m is the same as that introduced in the paragraph containing Eq. (87) (note that K_m depends on $\hat{r}_c$). The curves in Fig. 10(a) correspond to the type (i), the curves in Fig. 11(a) and the curves $p_1/p_0=6$ and 10 in Figs. 10(b) and 11(b) to the type (ii), and the curves $p_1/p_0=2$ and 4 in Figs. 10(b) and 11(b) to the type (iii).

The qualitative feature of the flow discussed in the present example remains true also when the porous slab is replaced by a channel or a pipe. In fact, essentially the same analytical expression for the mass-flow rate as Eq. (85) has been obtained in the case of pipe by Sharipov and Seleznev.[46]

V. CONCLUSION

In this paper, we have considered a steady rarefied gas flow over an in-line array of circular cylinders on the basis of the BGK equation and the diffuse reflection boundary condition on the cylinders. First, we have considered a steady rarefied gas flow in a periodic porous medium kept at a uniform temperature. We have derived, by homogenization, a fluid model that describes the global pressure distribution as well as the mass-flow rate (Sec. II). The derived model contains an effective diffusion tensor which is given by the mass-flow rate resulting from an associated elementary flow problem. For the case of an in-line array of circular cylinders, this problem is equivalent to investigating a flow of rarefied gas around infinitely many circular cylinders induced by a small uniform pressure gradient. We have solved this problem numerically and prepared the numerical data for the mass-flow rate (Sec. III). The derived model has a simple form and can be used as a practical tool. A simple application of the derived model to an isothermal flow through an array of circular cylinders induced by a pressure difference is presented in Sec. IV.

ACKNOWLEDGMENTS

S.T. expresses his cordial thanks to Professor Kazuo Aoki for his valuable advice and encouragement. He also thanks Professor Shigeru Takata for his interest and valuable comments. The present work was supported by the Grant-in-Aid for Scientific Research (No. 19760118) from the Japan Society for the Promotion of Science.

APPENDIX A: RELATION TO THE KLINKENBERG'S LAW

According to Klinkenberg,[75] the effective permeability K_g for low pressure gas flows through isotropic porous media is given by

$$K_g = K\left(1 + \frac{b}{p}\right), \tag{A1}$$

where K is the absolute permeability constant which depends only on the material, p is the pressure of the gas, and b is called the Klinkenberg factor. The coefficients $M_{P(0)}$ and $k_0\hat{M}_{P(1)}$ in Eq. (78) are related to the coefficients K and b in Eq. (A1), and the relation is as follows:

$$K = -M_{P(0)}\ell^2, \tag{A2}$$

$$b = k_0\frac{\hat{M}_{P(1)}}{M_{P(0)}}\frac{\mu(2RT_0)^{1/2}}{\ell}, \tag{A3}$$

where μ is the viscosity. Thus, b is proportional to k_0. Here, we have identified the pressure p as the leading order term of the expansion (17), i.e., $p = p_*\hat{p}_{(0)}$.

[1] M. N. Kogan, *Rarefied Gas Dynamics* (Plenum, New York, 1969).
[2] C. Cercignani, *The Boltzmann Equation and Its Applications* (Springer-Verlag, Berlin, 1988).
[3] C. Cercignani, *Rarefied Gas Dynamics, From Basic Concepts to Actual Calculations* (Cambridge University Press, Cambridge, 2000).
[4] Y. Sone, *Kinetic Theory and Fluid Dynamics*, "Modeling and Simulation in Science, Engineering and Technology" (Birkhäuser, Boston, 2002).
[5] Y. Sone, *Molecular Gas Dynamics: Theory, Techniques, and Applications* (Birkhäuser, Boston, 2006).
[6] G. M. Karniadakis and A. Beskok, *Micro Flows: Fundamentals and Simulation* (Springer-Verlag, New York, 2002).
[7] G. Karniadakis, A. Beskok, and N. Aluru, *Microflows and Nanoflows: Fundamentals and Simulation* (Springer Science+Business Media, New York, 2005)
[8] C. Cercignani, *Slow Rarefied Flows: Theory and Application to Micro-Electro-Mechanical Systems* (Birkhäuser, Basel, 2006).
[9] N. G. Hadjiconstantinou, "The limits of Navier–Stokes theory and kinetic extensions for describing small-scale gaseous hydrodynamics," Phys. Fluids **18**, 111301 (2006).
[10] E. H. Kennard, *Kinetic Theory of Gases* (McGraw-Hill, New York, 1938).
[11] Y. Sone, "Thermal creep in rarefied gas," J. Phys. Soc. Jpn. **21**, 1836 (1966).
[12] Y. Sone and K. Yamamoto, "Flow of rarefied gas through a circular pipe," Phys. Fluids **11**, 1672 (1968).
[13] T. Ohwada, Y. Sone, and K. Aoki, "Numerical analysis of the shear and thermal creep flows of a rarefied gas over a plane wall on the basis of the linearized Boltzmann equation for hard-sphere molecules," Phys. Fluids A **1**, 1588 (1989).
[14] T. Ohwada, Y. Sone, and K. Aoki, "Numerical analysis of the Poiseuille and thermal transpiration flows between two parallel plates on the basis of the Boltzmann equation for hard-sphere molecules," Phys. Fluids A **1**, 2042 (1989).
[15] Y. Sone, "Flows induced by thermal stress in rarefied gas," Phys. Fluids **15**, 1418 (1972).
[16] Y. Sone, in *Annual Review of Fluid Mechanics* (Annual Reviews, Palo Alto, 2000), p. 779.
[17] M. N. Kogan, V. S. Galkin, and O. G. Fridlender, "Stresses produced in gases by temperature and concentration inhomogeneities. New type of free convection," Sov. Phys. Usp. **19**, 420 (1976).
[18] K. Aoki, Y. Sone, and N. Masukawa, in *Rarefied Gas Dynamics*, edited by J. Harvey and G. Lord (Oxford University Press, Oxford, 1995), p. 35.
[19] Y. Sone and M. Yoshimoto, "Demonstration of a rarefied gas flow induced near the edge of a uniformly heated plate," Phys. Fluids **9**, 3530 (1997).
[20] H. Sugimoto and Y. Sone, in *Rarefied Gas Dynamics*, edited by M. Capitelli (AIP, Melville, 2005), p. 168.
[21] M. Knudsen, "Eine revision der gleichgewichtsbedingung der gase. Thermische Molekularströmung," Ann. Phys. **31**, 205 (1910).
[22] M. Knudsen, "Thermischer molekulardruck der gase in röhren," Ann. Phys. **33**, 1435 (1910).
[23] G. Pham-Van-Diep, P. Keeley, E. P. Muntz, and D. P. Weaver, in *Rarefied Gas Dynamics*, edited by J. Harvey and G. Lord (Oxford University Press, Oxford, 1995), p. 715.
[24] Y. Sone, Y. Waniguchi, and K. Aoki, "One-way flow of a rarefied gas induced in a channel with a periodic temperature distribution," Phys. Fluids **8**, 2227 (1996).
[25] S. E. Vargo and E. P. Muntz, in *Rarefied Gas Dynamics*, edited by C. Shen (Peking University Press, Peking, 1997), p. 995.
[26] M. L. Hudson and T. J. Bartel, in *Rarefied Gas Dynamics*, edited by R. Brun, R. Campargue, R. Gatignol, and J.-C. Lengrand (Cépaduès-Éditions, Toulouse, 1999), Vol. 1, p. 719.
[27] Y. Sone and K. Sato, "Demonstration of a one-way flow of a rarefied gas induced through a pipe without average pressure and temperature gradients," Phys. Fluids **12**, 1864 (2000).
[28] K. Aoki, Y. Sone, S. Takata, K. Takahashi, and G. A. Bird, in *Rarefied Gas Dynamics*, edited by T. J. Bartel and M. A. Gallis (AIP, Melville, 2001), p. 940.
[29] Y. Sone, T. Fukuda, T. Hokazono, and H. Sugimoto, in *Rarefied Gas Dynamics*, edited by T. J. Bartel and M. A. Gallis (AIP, Melville, 2001), p. 948.
[30] Y. Sone and H. Sugimoto, in *Rarefied Gas Dynamics*, edited by E. P. Muntz and A. Ketsdever (AIP, Melville, 2003), p. 1041.
[31] Y. L. Han, M. Young, E. P. Muntz, and G. Shiflett, in *Rarefied Gas Dynamics*, edited by M. Capitelli (AIP, Melville, 2005), p. 162.
[32] M. Young, Y. L. Han, E. P. Muntz, and G. Shiflett, in *Rarefied Gas Dynamics*, edited by M. Capitelli (AIP, Melville, 2005), p. 174.
[33] K. Aoki and P. Degond, "Homogenization of a flow in a periodic channel of small section," Multiscale Model. Simul. **1**, 304 (2003).
[34] K. Aoki, P. Degond, S. Takata, and H. Yoshida, "Diffusion models for Knudsen compressors," Phys. Fluids **19**, 117103 (2007).

[35]S. Takata, H. Sugimoto, and S. Kosuge, "Gas separation by means of the Knudsen compressor," Eur. J. Mech. B/Fluids **26**, 155 (2007).
[36]M. Kayashima, Japan Patent No. 1513106 (27 July 1984).
[37]P. L. Bhatnagar, E. P. Gross, and M. Krook, "A model for collision processes in gases. I. Small amplitude processes in charged and neutral one-component systems," Phys. Rev. **94**, 511 (1954).
[38]P. Welander, "On the temperature jump in a rarefied gas," Ark. Fys. **7**, 507 (1954).
[39]M. N. Kogan, "On the equations of motion of a rarefied gas," Appl. Math. Mech. **22**, 597 (1958).
[40]P. Charrier and B. Dubroca, "Asymptotic transport models for heat and mass transfer in reactive porous media," Multiscale Model. Simul. **2**, 124 (2003).
[41]A. Bensoussan, J. L. Lions, and G. Papanicolaou, *Asymptotic Analysis for Periodic Structures* (North-Holland, Amsterdam, 1978).
[42]E. W. Larsen, "Neutron transport and diffusion in inhomogeneous media. I," J. Math. Phys. **16**, 1421 (1975); "Neutron transport and diffusion in inhomogeneous media. II," Nucl. Sci. Eng. **60**, 357 (1976).
[43]L. Dumas and F. Golse, "Homogenization of transport equations," SIAM J. Appl. Math. **60**, 1447 (2000).
[44]T. Goudon and F. Poupaud, "Approximation by homogenization and diffusion of kinetic equations," Commun. Partial Differ. Equ. **26**, 537 (2001).
[45]S. Fukui and R. Kaneko, "Analysis of ultra-thin gas film lubrication based on linearized Boltzmann equation: First report-derivation of a generalized lubrication equation including thermal creep flow," J. Tribol. **110**, 253 (1988).
[46]F. M. Sharipov and V. D. Seleznev, "Rarefied gas flow through a long tube at any pressure ratio," J. Vac. Sci. Technol. A **12**, 2933 (1994).
[47]F. Sharipov, "Rarefied gas flow through a long tube at any temperature ratio," J. Vac. Sci. Technol. A **14**, 2627 (1996).
[48]C. Cercignani, M. Lampis, and S. Lorenzani, in *Rarefied Gas Dynamics*, edited by M. Capitelli (AIP, Melville, 2005), p. 719.
[49]C. Shen, "Use of the degenerated Reynolds equation in solving the microchannel flow problem," Phys. Fluids **17**, 046101 (2005).
[50]E. A. Mason and A. P. Malinauskas, *Gas Transport in Porous Media: The Dusty-Gas Model* (Elsevier, Amsterdam, 1983).
[51]A. A. Shapiro, "A kinetic theory of the filtration of rarified gas in an anisotropic porous media," Theor. Found. Chem. Eng. **27**, 140 (1993).
[52]L. M. de Socio, N. Ianiro, and L. Marino, "A model for the compressible flow through a porous medium," Math. Models Meth. Appl. Sci. **11**, 1273 (2001).
[53]V. Pavan and L. Oxarango, "A new momentum equation for gas flow in porous media: The Klinkenberg effect seen through the kinetic theory," J. Stat. Phys. **126**, 355 (2006).
[54]H. Babovsky, "On Knudsen flows within thin tubes," J. Stat. Phys. **44**, 865 (1986).
[55]H. Babovsky, C. Bardos, and T. Platkowski, "Diffusion approximation for a Knudsen gas in a thin domain with accommodation on the boundary," Asymptotic Anal. **3**, 265 (1991).
[56]C. Börgers, C. Greengard, and E. Thomann, "The diffusion limit of free molecular flow in thin plane channels," SIAM J. Appl. Math. **52**, 1057 (1992).
[57]F. Golse, "Anomalous diffusion limit for the Knudsen gas," Asymptotic Anal. **17**, 1 (1998).
[58]C. Bardos, L. Dumas, and F. Golse, "Diffusion approximation for billiards with totally accommodating scatters," J. Stat. Phys. **86**, 351 (1997).
[59]Y. Sone and S. Takata, "Discontinuity of the velocity distribution function in a rarefied gas around a convex body and the S layer at the bottom of the Knudsen layer," Transp. Theory Stat. Phys. **21**, 501 (1992).
[60]Y. Sone, "New kind of boundary layer over a convex solid boundary in a rarefied gas," Phys. Fluids **16**, 1422 (1973).
[61]H. Sugimoto and Y. Sone, "Numerical analysis of steady flows of a gas evaporating from its cylindrical condensed phase on the basis of kinetic theory," Phys. Fluids A **4**, 419 (1992).
[62]Y. Sone and H. Sugimoto, "Kinetic theory analysis of steady evaporating flows from a spherical condensed phase into a vacuum," Phys. Fluids A **5**, 1491 (1993).
[63]S. Takata, Y. Sone, and K. Aoki, "Numerical analysis of a uniform flow of a rarefied gas past a sphere on the basis of the Boltzmann equation for hard-sphere molecules," Phys. Fluids A **5**, 716 (1993).
[64]Y. Sone, S. Takata, and M. Wakabayashi, "Numerical analysis of a rarefied gas flow past a volatile particle using the Boltzmann equation for hard-sphere molecules," Phys. Fluids **6**, 1914 (1994).
[65]Y. Sone and H. Sugimoto, "Evaporation of a rarefied gas from a cylindrical condensed phase into a vacuum," Phys. Fluids **7**, 2072 (1995).
[66]S. Takata and Y. Sone, "Flow induced around a sphere with a nonuniform surface temperature in a rarefied gas, with application to the drag and thermal force problems of a spherical particle with an arbitrary thermal conductivity," Eur. J. Mech. B/Fluids **14**, 487 (1995).
[67]M. Abramowitz and I. A. Stegun, *Handbook of Mathematical Functions with Formulas, Graphs, and Mathematical Tables* (Dover, New York, 1972), p. 1001.
[68]K. Aoki, Y. Sone, and T. Yano, "Numerical analysis of a flow induced in a rarefied gas between noncoaxial circular cylinders with different temperatures for the entire range of the Knudsen number," Phys. Fluids A **1**, 409 (1989).
[69]Y. Sone, in *Rarefied Gas Dynamics*, edited by L. Trilling and H. Y. Wachman (Academic, New York, 1969), Vol. 1, p. 243.
[70]Y. Sone and K. Yamamoto, "Flow of rarefied gas over plane wall," J. Phys. Soc. Jpn. **29**, 495 (1970); see also Y. Sone and Y. Onishi, *ibid.* **47**, 672 (1979).
[71]Y. Sone, in *Rarefied Gas Dynamics*, edited by D. Dini (Editrice Tecnico Scientfica, Pisa, 1971), Vol. 2, p. 737.
[72]Y. Sone, in *Advances in Kinetic Theory and Continuum Mechanics*, edited by R. Gatignol and Soubbaramayer (Springer-Verlag, Berlin, 1991), p. 19.
[73]Y. Sone, K. Aoki, S. Takata, H. Sugimoto, and A. V. Bobylev, "Inappropriateness of the heat-conduction equation for description of a temperature field of a stationary gas in the continuum limit: Examination by asymptotic analysis and numerical computation of the Boltzmann equation," Phys. Fluids **8**, 628 (1996); **8**, 841 (E) (1996).
[74]Y. Sone, C. Bardos, F. Golse, and H. Sugimoto, "Asymptotic theory of the Boltzmann system, for a steady flow of a slightly rarefied gas with a finite Mach number: General theory," Eur. J. Mech. B/Fluids **19**, 325 (2000).
[75]L. J. Klinkenberg, in *Drilling and Production Practice* (American Petroleum Institute, New York, 1941), p. 200.